Inorganic Chemistry

pubs.acs.org/IC

Article

Mechanisms of Alcohol Oxidation Catalyzed by Co(III)-Oxo Cubanes: A Computational Study

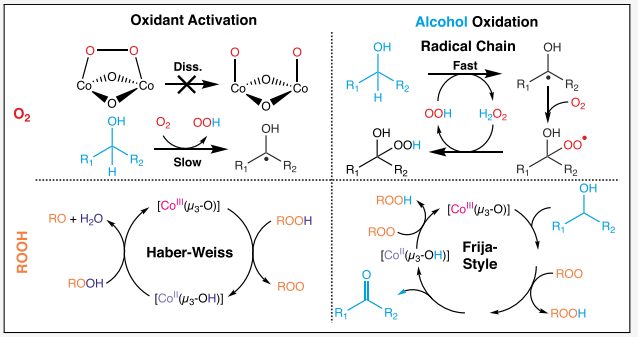
Niklas Sülzner,* Melanie Alexandra Cedeño Manrique, and Christof Hättig

Cite This: https://doi.org/10.1021/acs.inorgchem.6c03033

Read Online

ACCESS | Metrics & More | Article Recommendations | Supporting Information

ABSTRACT: We present a computational study on the reaction mechanisms for thermal alcohol oxidation at Co-oxo cubane [Co_4O_4] complexes in acetonitrile solution, using hybrid DFT in combination with DCOSMO-RS. These complexes serve as molecularly well-defined models for the interfacial reactivity of extended Co oxide surfaces. A key focus is placed on comparing different possible reaction pathways to obtain a detailed mechanistic picture. To this end, the alcohols *iso*-propanol and benzyl alcohol, together with the oxidants O_2, H_2O_2, and *tert*-butyl hydroperoxide, are selected as model systems. Clear mechanistic differences are observed between oxidation with O_2 and the hydroperoxides (ROOH). For ROOH, two catalytic cycles are identified: one for ROOH decomposition, generating ROO•, and one for alcohol oxidation, consuming ROO•. In contrast, for O_2, no efficient activation via homolytic pathways with reasonable energy barriers is found, suggesting that alcohol oxidation with O_2 may additionally involve radical chain processes. Overall, the calculations indicate a strong preference for homolytic over heterolytic pathways. For the cobalt atoms, we find that oxidation states higher than IV do not appear to play a significant role.



INTRODUCTION

Liquid-phase oxidation has emerged as a highly relevant area in industrial chemistry for the production of fine chemicals under mild conditions.[1,2] To improve sustainability and reduce production costs, so-called green oxidants such as molecular oxygen (O_2), hydrogen peroxide (H_2O_2), and *tert*-butyl hydroperoxide (TBHP) are preferred over costly and toxic inorganic oxidants that generate environmentally problematic waste (e.g., containing Mn or Cr).[3] Moreover, the development of cost-efficient catalysts tailored to these liquid-phase oxidations is essential, where oxides of the earth-abundant transition metals iron or cobalt are promising.[4] Among cobalt-based materials, perovskites (e.g., $LaCo_{1-x}Fe_xO_3$) and spinels (e.g., $Co_{3-x}Fe_xO_4$) have attracted considerable attention, as they are widely used as catalysts in the selective thermal oxidation of alcohols,[5−11] as well as olefin epoxidation reactions.[12−16] While these materials are inexpensive and readily available, they often exhibit low activity in their pristine form without further modifications.[17] Enhancing their catalytic performance through rational design remains a key challenge,[18,19] which requires a detailed mechanistic understanding of their reactivity.

Despite numerous studies on the use of transition metal oxides (TMOs) as oxidation catalysts, mechanistic insight often remains elusive because important intermediates are transient, which complicates their spectroscopic characterization and assignment. Most mechanistic studies are restricted to conversion, yield, selectivity, and apparent reaction kinetics, while only limited information on the individual elementary steps and intermediates is available. In particular, the identification of the active species, especially the oxidation states of the metal centers, is of central importance. A notable counterexample that provides detailed mechanistic insight is the recent study by Hareendran et al. on the oxidation of cyclohexane with O_2 over $LaCo_{1-x}Fe_xO_3$ perovskites.[20] In a comprehensive approach combining kinetic experiments, EPR spectroscopy, surface characterization, and theory, the oxidative role of Co^{III} and its involvement in the decomposition of a hydroperoxide intermediate via a Haber-Weiss cycle were elucidated.

In the context of liquid-phase alcohol oxidation, *iso*-propanol (*i*-PrOH), benzyl alcohol (BnOH), and cinnamyl alcohol (CnOH) in combination with O_2, H_2O_2, and TBHP are commonly employed as model systems to investigate reaction mechanisms.[9−11,16,21] Most studies, however, are limited to identifying general trends. For example, the oxidation of CnOH with TBHP over $LaCo_{1-x}Fe_xO_3$ involves reactive oxygen species (ROS) in solution, along with an induction

Received: June 11, 2026
Revised: August 17, 2026
Accepted: August 21, 2026

ACS Publications © XXXX American Chemical Society

Downloaded from pubs.acs.org/inocaj/article-pdf/doi/10.1021/acs.inorgchem.6c03033/6828356/acs.inorgchem.6c03033.pdf by RUHR UNIVERSITAET BOCHUM user on 03 September 2026

period associated with TBHP decomposition and ROS formation.[10] For the oxidation of *i*-PrOH with O_2 over $Co_{3-x}Fe_xO_4$, ensembles of Co^{3+} have been identified as the active species.[9] In the case of BnOH, styrene, and CnOH oxidation, Fe doping significantly affects the activity of $Co_{3-x}Fe_xO_4$, with distinct differences between the oxidants O_2 and TBHP.[11] In addition, both uncatalyzed and (transition-metal) catalyzed thermal decomposition of TBHP have been extensively investigated.[22−27] These studies indicate that spin-state changes are important for reactions with O_2, which has a triplet ground state, whereas for reactions with TBHP, partial decomposition of the latter is rate-determining.

To obtain more detailed mechanistic information, molecular model systems like Co-oxo heterocubane complexes ($[Co_4O_4]$) provide a promising approach, as they are accessible to spectroscopic and analytical techniques that are not readily applicable to nanoparticle surfaces. However, this advantage comes at the trade-off that such systems are similar to low-nuclear inorganic compounds and, thus, the transferability of insights to extended materials must be carefully assessed. The complex $[Co_4O_4(OAc)_2(bpy)_2]$ (OAc: acetate; bpy: bipyridine), first isolated by Dimitrou et al.,[28] resembles a structural fragment of Co_3O_4 featuring Co^{III} centers in octahedral coordination (cf. Figure 1). As such, these complexes occupy a unique position between extended TMOs and small mono- or dinuclear transition metal complexes.

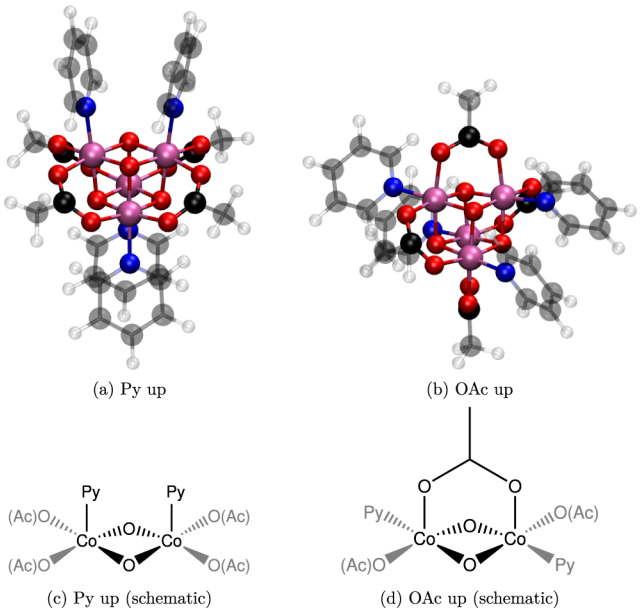


Figure 1. Molecular structure of complex **1**, $[Co_4^{III}O_4(OAc)_4(py)_4]$ (Ac = $OCCH_3$), used in this work. (a−b) Orientations with either the Py (a) or OAc (b) ligands pointing upward and the $[Co_4O_4]$ core and nearest coordination partners highlighted. (c−d) Corresponding representations for the upper $[Co_2O_2]$ facet in which the lower facet and remaining ligands are omitted for clarity.

$[Co_4^{III}O_4]^{4+}$ has been extensively studied as a catalyst for oxygen evolution in electrochemical water oxidation, e.g., by the groups of Tilley[29−31] and Nocera,[32−34] as reviewed recently in ref 35. Under these electrochemical conditions, the singly $[Co_3^{III}Co^{IV}O_4]^{5+}$ and doubly oxidized species, formally $[Co_2^{III}Co_2^{IV}O_4]^{6+}$ or $[Co_3^{III}Co^{V}O_4]^{6+}$, have been identified.[32−34] Via a modification of the original procedure by Beattie et al.,[36] Chakrabarty and Das developed a more controlled synthetic route to $[Co_4^{III}O_4(O_2CR)_4(L)_4]$, providing facile access to derivatives that differ in the carboxylate (O_2CR) and pyridine (L) ligands.[37,38] The same authors also investigated the use of these complexes in thermal catalysis for liquid-phase oxidation of organic substrates, including the systems *α*-pinene/O_2,[37,39,40] styrene/TBHP,[41] ethylbenzene/O_2 and *p*-xylene/O_2,[38,40,42] benzylic and secondary alcohols with TBHP,[43,44] and diphenylmethane with TBHP, H_2O_2, and NaOCl.[41] Despite these numerous studies, only limited mechanistic information—largely restricted to speculations based on simple control experiments—is available.

Until recently, only two studies have investigated the reaction mechanisms of oxidation reactions catalyzed by $[Co_4O_4]$, of which only one considered alcohol oxidation.[45,46] Lee et al. investigated olefin oxidation with *meta*-chloroperoxybenzoic acid at a related $[Co_4^{II}(OH)_4]^{4+}$ catalyst, which is assumed to be initially oxidized to $[Co_4^{III}O_4]^{4+}$.[45] They observed a competition between homolytic and heterolytic pathways in the decomposition of a central (per)oxyl intermediate that determines the product distribution: heterolysis involving a Co^{V} species leads to epoxidation (80%), whereas homolysis involving a Co^{IV} species results in allylic oxidation (20%). For other lower-nuclear complexes (e.g., mononuclear $Cr^{VI}O_3$ and Cu^{II} or a heterobimetallic Co−Al complex),[47−49] it has been shown that the oxidation of benzyl alcohol with TBHP proceeds heterolytically, involving higher oxidation states via metal-oxo pathways, rather than peroxyl metal pathways. Gutiérrez-Tarriño et al. studied cyclohexane oxidation with O_2 and found a radical chain mechanism with cyclohexyl hydroperoxide (CHHP) as a key intermediate.[46] The catalyst plays in this case a dual role, assisting both in the activation of O_2 and in the decomposition of CHHP. Similar effects regarding hydroperoxide decomposition have been observed for CHHP at $LaCo_{1-x}Fe_xO_3$ perovskite materials by Hareendran et al.,[20,50,51] and for cyclohexenyl hydroperoxide involved in cyclohexene oxidation at related transition metal oxides by Büker et al.[12−16]

Recently, some of us provided computational evidence for the assignment of characteristic features of $[Co_4^{III}O_4(O_2CR)_4(py)_4]$ (py: pyridine) with R = Me (**1**), Et (**2**), and *i*-Pr (**3**) in IR and UV/vis spectroscopy.[52] Moreover, in a collaboration combining kinetic analysis, EPR characterization, and theory, the oxidation mechanisms of *i*-PrOH, BnOH, and CnOH with O_2, H_2O_2, and TBHP at complexes **1** and **2** as catalysts were investigated.[53] For the oxidations with hydroperoxide (ROOH) oxidants, it was proposed that two interrelated catalytic cycles are at play: (1) A Haber-Weiss activation of ROOH involving homolytic bond cleavages and a Co^{II} intermediate, generating alkyl oxyl ($RO^{\bullet}$) and alkyl peroxyl ($ROO^{\bullet}$) radicals; (2) Stepwise oxidation of the alcohol by $ROO^{\bullet}$ in a homolytic mechanism, close to that found by Frija et al. at mononuclear Cu^{II} and Co^{II} catalysts.[54,55]

However, no insight into how the electronic structure of the catalyst affects the stability and reactivity of key intermediates nor information on the reaction mechanisms for O_2 activation or on alcohol oxidation with O_2 have been provided. Moreover, a comparison to other possible reaction pathways has not been made. To address these gaps, the present work provides a computational study on the mechanistic details of alcohol oxidation at the $[Co_4O_4]$ complex **1** (see Figure 1). A

Downloaded from pubs.acs.org/inocaj/article-pdf/doi/10.1021/acs.inorgchem.6c03033/6828356/acs.inorgchem.6c03033.pdf by RUHR UNIVERSITAET BOCHUM user on 03 September 2026

https://doi.org/10.1021/acs.inorgchem.6c03033
Inorg. Chem. XXXX, XXX, XXX−XXX

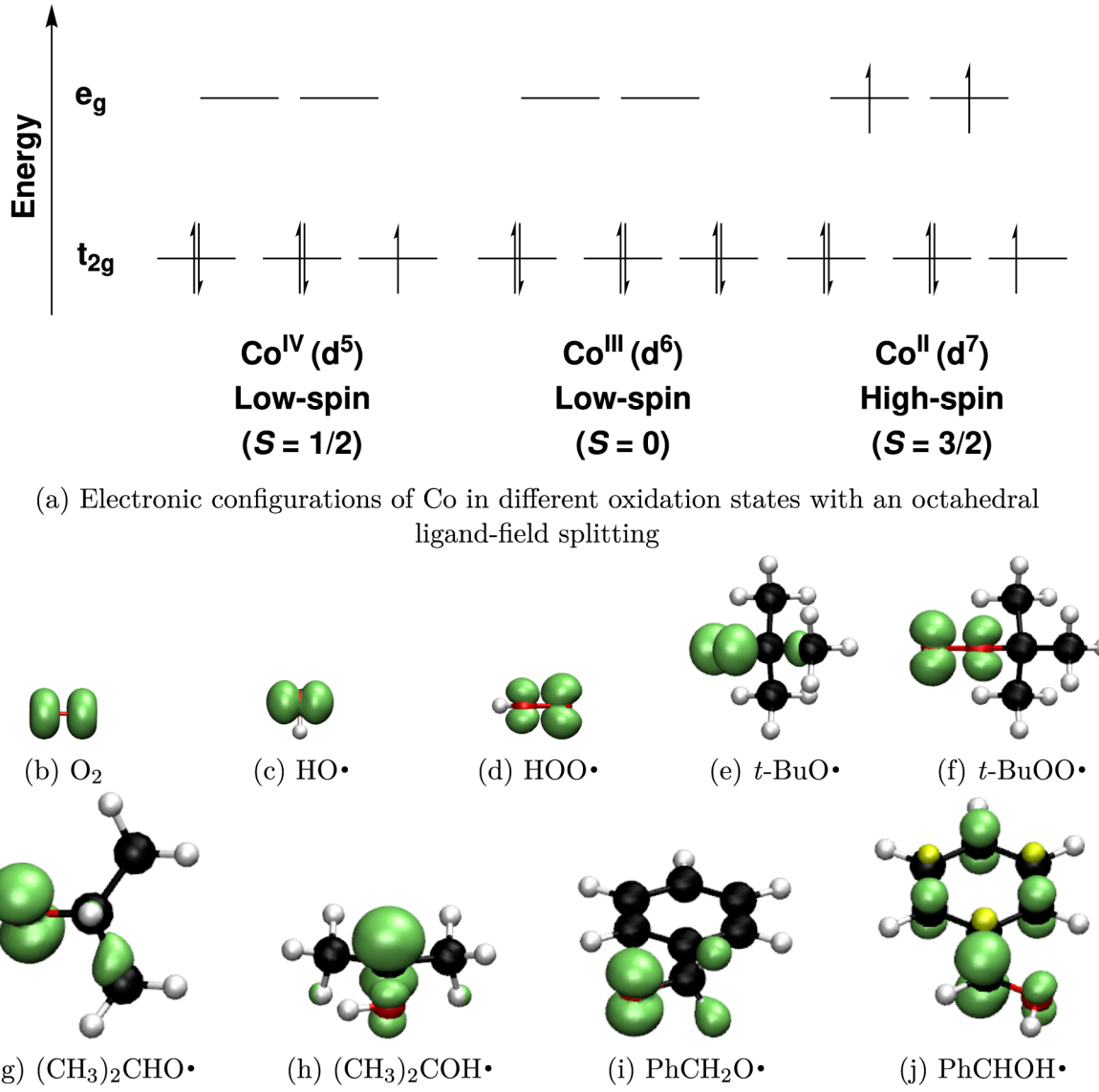


Figure 2. Electronic configurations of Co (a) and spin densities of relevant radical species (b–j) in this study.

key focus is placed on the comparison of different possible reaction pathways and on the electronic structure of the involved intermediates. We address key questions regarding (i) ligand substitution (acetate vs pyridine), (ii) the reaction site (in solution vs at the catalyst), (iii) the oxidation states, and (iv) the nature of bond breaking (homolytic vs heterolytic). Thereby, we elucidate the electronic structure and the energetic and kinetic reasons behind the role of the catalyst and for the differences in reactivity observed for O_2, H_2O_2, and TBHP as oxidants.

■ COMPUTATIONAL DETAILS

General Information

All DFT calculations were done with the TURBOMOLE program package version 7.9,[56,57] employing the resolution-of-the-identity approximation for the Coulomb potential (RI-J). Structures were optimized in solution using DFT (modules ridft and rdgrad)[58−60] with the PBE0[61−63] functional, the def2-TZVP basis sets[58,64] and the standard TURBOMOLE numerical integration grid (gridsize 4), as defined by Treutler and Ahlrichs,[59] combined with the conductor-like screening model (COSMO)[65,66] as an implicit solvent model. COSMO was used with settings for acetonitrile (relative dielectric constant ϵ_r = 37.5), the Gaussian charge model,[67] and default settings for the cavity construction. The augmented Roothaan-Hall method was used for the MO optimization.[68] Default convergence thresholds were used for the MOs (SCF energy convergence: 10^{-7}; density matrix convergence: 10^{-6}) and during the structure optimization (energy convergence: 10^{-6}; Cartesian gradient convergence: 10^{-3}). All molecular structures together with their DFT energies are available in a data publication on Zenodo.[69] Energy diagrams were plotted with help of the Python application mechaSVG.[70]

Unrestricted Kohn−Sham (UKS) calculations were used for all open-shell species. Organic radical species with a single unpaired electron were calculated with M_S = 1/2 for a doublet (S = 1/2) configuration in UKS. For closed-shell structures involving $[Co_4^{III}O_4]^{4+}$, we exploited the known closed-shell low-spin (S = 0) configuration of Co^{III} in these complexes.[36,44] Complexes involving other Co oxidation states (cf. Figure 2(a)) were assumed to have high-spin configurations for Co^{II} and low-spin configurations for Co^{IV} and Co^{V}, in line with the

Downloaded from pubs.acs.org/inocaj/article-pdf/doi/10.1021/acs.inorgchem.6c03033/6828356/acs.inorgchem.6c03033.pdf by RUHR UNIVERSITAET BOCHUM user on 03 September 2026

https://doi.org/10.1021/acs.inorgchem.6c03033
Inorg. Chem. XXXX, XXX, XXX−XXX

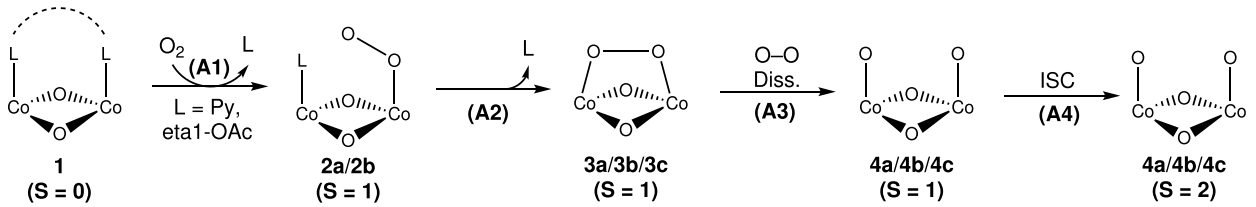


Figure 3. Reaction scheme for the activation of O_2 at $[Co_4O_4]$ (cf. energies in Table 1) [L = Py (a), η_1-OAc (b), η_2-OAc (c)].

literature on $[Co_3^{III}Co^{V}O_4]^{6+}$ (S = 1)[29] and $[Co_3^{III}Co^{IV}O_4]^{5+}$ (S = 1/2).[32] The validity of the high-spin assumption for $[Co^{II}Co_3^{III}O_4]^{3+}$ has been confirmed by EPR spectroscopy.[53] The possibility for spin changes during the chemical reactions was accounted for by investigating multiple spin states where meaningful. Unless stated explicitly, the reaction mechanisms are based on pathways with lowest barriers. All calculations were carefully checked for spin contamination based on the $\langle S^2 \rangle$ expectation values (see Table S1). Information on the oxidation states of the relevant atoms (particularly Co) was determined based on analysis of the intrinsic bond orbitals (IBOs)[71] and the UKS spin density (contour values of ± 0.01 au used in the plots). For reference, the spin density of the most relevant organic radicals are shown in Figure 2(b–j). In the following, we use for spin states the short hand notation S (S = 0), D (S = 1/2), T (S = 1), and Q (S = 3/2). Higher spin states are denoted by specifying the value of S.

Total Energies

Harmonic frequencies were calculated at the COSMO–DFT/PBE0/def2-TZVP level using analytic Hessians (with the aoforce module)[72] and used in the calculation of zero-point vibrational energy (ZPVE) corrections to the electronic energies. Structure optimizations and frequency calculations included the contributions from the derivatives of integration weights. Final electronic energies were calculated at the COSMO–DFT/PBE0/def2-TZVP geometries with the direct COSMO-RS (DCOSMO-RS)[73,74] method, i.e., a self-consistent implementation of COSMO-RS (COSMO for real solvents)[66,75] that goes beyond the pure electrostatic picture, using settings for acetonitrile (ϵ_r = 37.5) as the solvent from the experiments in ref 53. The COSMO-RS σ potential of acetonitrile needed for the DCOSMO-RS calculations was taken from the TURBOMOLE version 7.9 release and had been derived with the COSMOtherm program using the BP_TZVP_C21_0111 parametrization at 25 °C and infinite dilution of the solute.[76]

The effect of DCOSMO-RS on the structures is small and was therefore neglected (cf. Table S2). DCOSMO-RS energies used here do neither include outlying charge corrections nor the combinatorial contribution of the solute. Unless stated otherwise, all reported reaction and activation energies were computed as the sum of the DCOSMO-RS electronic energies and the COSMO–DFT/PBE0/def2-TZVP ZPVEs. As an alternative to PBE0, single-point electronic energies were also calculated at the existing geometries using the long-range separated functional LC-wPBE[77] combined with DCOSMO-RS. The corresponding ZPVE-corrected LC-wPBE results are given in Tables S3–S23 for all reaction paths discussed in the main text. No qualitative differences between PBE0 and LC-wPBE were observed, neither in the energies, nor regarding spin contamination (cf. Table S1).

Free Energies

For a better comparison with the experimental kinetic studies in ref 53., Helmholtz free reaction and activation energies

$$\Delta A = \Delta U - T\Delta S \quad (1)$$

were additionally calculated. ΔU are the ZPVE-corrected DCOSMO-RS-DFT/def2-TZVP energies described above for either PBE0 or LC-wPBE. The entropic contributions (ΔS) were calculated using the rigid-rotor–harmonic-oscillator model at temperature T and pressure p (using freeh) based on the harmonic frequencies calculated at the COSMO–DFT/PBE0/def2-TZVP level. In accordance with the experiments, three conditions (T, p) were selected:

- 25 °C, 1 bar: Standard conditions
- 82 °C, 1 bar: Experimental conditions for H_2O_2 and TBHP
- 150 °C, 10 bar: Experimental condition for O_2

Free energies of solvation were not explicitly taken into account since all quantities already refer to the results in (implicit) solution.

RESULTS AND DISCUSSION

O_2 Activation

The initial steps of a possible activation of O_2 at the $[Co_4O_4]$ complex (see Figures 3 and S24 and Table 1) involve O_2 binding to the complex, which requires free coordination sites at the Co centers. Different pathways leading to complexes with either two pyridine ligands removed (a), two acetate ligands reduced in hapticity from η_2 to η_1 (b), or one acetate

Table 1. Reaction Energies and Barriers (In Parentheses) (In kJ/mol) for the Activation of O_2 (Steps According to Figure 3)

Step	Description	Energy
A1	*End-on binding of O_2via*	
A1a	Elimination of one Py	67.6
A1b	Hapticity reduction ($\eta_2 \rightarrow \eta_1$) of one AcO^-	71.4
A2	*Conversion into side-on binding via*	
A2a	Elimination of another Py	178.9[a]
A2b	Hapticity reduction ($\eta_2 \rightarrow \eta_1$) of another AcO^-	125.5
A2c	Elimination of η_1-OAc^-	145.6
A3	*O–O Dissociation at*	
A3a	$[(\eta_2\text{-OAc})_4(py)_2(O_2)]$	148.6[a] (212.7)
A3b	$[(\eta_2\text{-OAc})_2(\eta_1\text{-OAc})_2(py)_4(O_2)]$	216.1[a] (204.0)
A3c	$[(\eta_2\text{-OAc})_3(py)_4(O_2)]$	191.0 (210.1)
A4	*ISC* (Triplet → Quintet) in	
A4a	$[(\eta_2\text{-OAc})_4(py)_2(\mu_1\text{-O})_2]$	−24.4
A4b	$[(\eta_2\text{-OAc})_2(\eta_1\text{-OAc})_2(py)_4(\mu_1\text{-O})_2]$	−26.2[a]
A4c	$[(\eta_2\text{-OAc})_3(py)_4(\mu_1\text{-O})_2]$	−22.2

[a]Estimate based on constraint structures.

https://doi.org/10.1021/acs.inorgchem.6c03033
Inorg. Chem. XXXX, XXX, XXX–XXX

Downloaded from pubs.acs.org/inocaj/article-pdf/doi/10.1021/acs.inorgchem.6c03033/6828356/acs.inorgchem.6c03033.pdf by RUHR UNIVERSITAET BOCHUM user on 03 September 2026

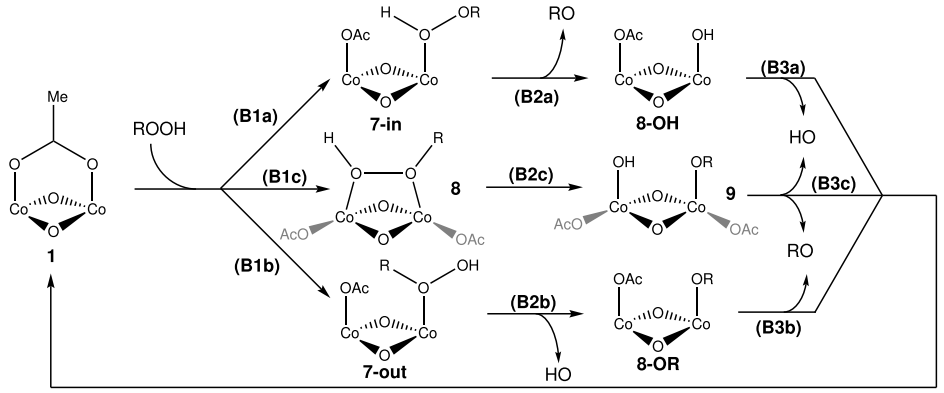


Figure 4. ROOH dissociation at $[Co_4O_4]$ (cf. energies in Table 2) involving $\eta_2 \rightarrow \eta_1$ hapticity reduction of a single (paths a and b; black) or two separate (path c; gray) OAc ligands.

ligand removed (c) are compared. Whereas the energy required for removal of the first pyridine (Py) is essentially identical to that for reduction of the hapticity of an acetate (OAc) ligand (ca. 70 kJ/mol), removal of a second Py does not yield a stable intermediate (**3a**) on the PBE0/def2-TZVP triplet surface, only on the surface for the smaller def2-SVP basis set. Instead, on the def2-TZVP triplet surface, the μ_2-O_2 in structure **3a** changes into μ_1-O_2, leaving one coordination site at Co open. The estimated def2-TZVP energy at the constraint structures for substitution of a second Py is significantly higher than for the first one, and higher than for further changes on the acetate ligands. Because of charge separation, elimination of the monodentate acetate (**3c**) is slightly disfavored compared to reduction in hapticity of another bidentate acetate (**3b**).

Minima for intermediates with a dissociated O−O bond were found on the PBE0/def2-TZVP triplet and quintet potential energy surfaces for complexes with either two Py ligands (**4a**) or one OAc ligand removed (**4c**). Structure **4b** was identified as a minimum only at the PBE0/def2-SVP level. As above, upper limits for the reaction energies were estimated by def2-TZVP single-point energies at def2-SVP geometries. The results indicate that formation of these structures would require to overcome an overall activation energy of approximately 400 kJ/mol. Following O−O bond dissociation, an intersystem crossing (ISC) from the triplet (S = 1) to the quintet (S = 2) state may occur, lowering the energy by approximately 20−25 kJ/mol. Details on the electronic structure of the O_2 complexes is given in the Supporting Information (Figures S1−S13).

Owing to the high barriers and largely endothermic reaction energies, the formation of the activated O_2 complexes **3** and **4** is highly unlikely under thermal conditions. In particular, the associated free energies under the experimental conditions (150 °C, 10 bar) in ref 53. are even slightly larger (cf. Table S3). Since the electronic structure of **2** is almost identical with O_2, that species is expected to be no more reactive than O_2, suffering from the same kinetic limitations. This is in line with a lack of experimental observations regarding thermal O_2 activation by $[Co_4O_4]$. Its reported participation under (photo)electrochemical conditions (water oxidation),[31,35,78−85] is assumed to involve higher-oxidized cobalt species.[29,30,32−34]

ROOH Activation

O−O Dissociation. For ROOH activation, we first consider a pathway with O−O bond dissociation of a single ROOH molecule at the catalyst (Figures 4 and S25, Table 2).

Table 2. Reaction Energies (In kJ/mol) for the ROOH Activation *via* O−O Dissociation (Steps According to Figure 4 and Plotted in Figure S25)

Step	Description	H_2O_2 (R = H)	TBHP (R = *t*-Bu)
B1	*ROOH addition*		
B1a	In	−17.9	−2.0
B1b	Out	−17.9	57.5
B1c	Side-on	113.5	123.3
B2	*O−O Homolysis into*		
B2a	[(HO)] and RO•	119.1	69.5
B2b	[(RO)] and HO•	119.1	110.7
B2c	[(RO)(HO)]	32.2	26.3
B3	*Elimination of*		
B3a	HO•	84.2	84.2
B3b	RO•	84.2	−16.4
B3c	HO• and RO•	39.7	2.1
B1−B3	ROOH → HO• + RO•	185.5	151.7

This mechanism consists of ROOH addition (1), the O−O homolysis (2), and radical elimination (3). We restrict the discussion of the addition and substitution steps to the OAc ligands due their similar energetic costs (cf. Table 1). Details on the electronic structure of the intermediates are given in the SI (Figures S26 and S15−S17). Three binding modes are considered (cf. Figure 4): binding via the OH group (*in* configuration; case a), via the RO group (*out* configuration; case b), and side-on binding via both O atoms (case c). Binding is more exothermic for H_2O_2 (−17.9 kJ/mol) than for TBHP (−2.0 kJ/mol), due to stronger hydrogen bonding (HB) to a nearby OAc ligand. For TBHP, where the *in* and *out* configurations differ significantly, a clear preference for the *in* configuration is observed. In contrast, the energetic cost of side-on binding is similar for both oxidants.

The above results show for TBHP a clear preference for pathway a (or for H_2O_2 the equivalent pathway b) up to the formation of intermediate **8-OH**. Due to high energetic costs of additional ca. 84 kJ/mol for the elimination of HO•, needed to close the catalytic cycle, the reaction scheme in Figure 4 alone cannot explain the catalytic peroxide decomposition. To become energetically feasible, it has to be combined with

Downloaded from pubs.acs.org/inocaj/article-pdf/doi/10.1021/acs.inorgchem.6c03033/6828356/acs.inorgchem.6c03033.pdf by RUHR UNIVERSITAET BOCHUM user on 03 September 2026

https://doi.org/10.1021/acs.inorgchem.6c03033
Inorg. Chem. XXXX, XXX, XXX−XXX

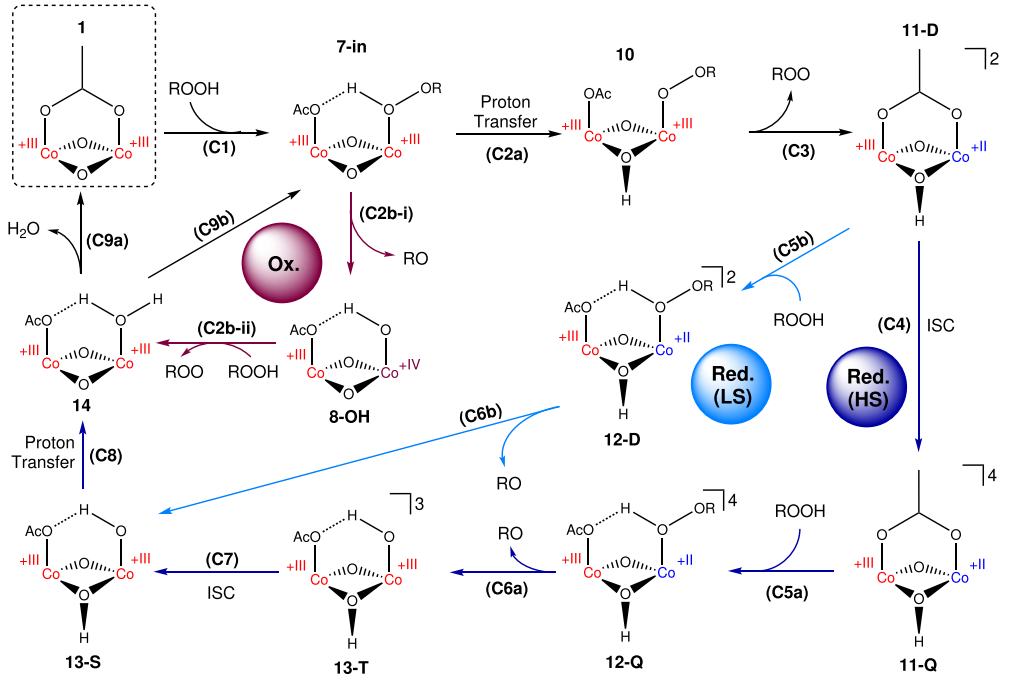


Figure 5. Haber-Weiss mechanism for the decomposition of ROOH with Co^{III} in red, Co^{IV} in brown, and Co^{II} in blue (energies given in Table 3). Oxidative pathway in brown, reductive low-spin (LS) pathway in light blue, and reductive high-spin (HS) pathway in dark blue.

reactions that regenerate the Co^{III} center and eliminate HO as HO^- or H_2O (*vide infra*).

Haber-Weiss Mechanism. Besides dissociation of the peroxo bond, ROOH can also be decomposed via hydrogen abstraction to form ROO• radicals. Combining this step with the first part of the mechanism discussed above such that one $HO^•$ radical remains bound to the catalyst until it has been reduced to H_2O, leads to a sequence of reactions commonly referred to in the literature as Haber-Weiss mechanism,[20,50,51,53] known, for example, for Cu or Fe ions as catalysts (e.g., in the seminal works of Fenton[86] or Haber and Weiss,[87] as well as detailed studies by Barton[22,23] and Kochi.[88−90]) Key features of this mechanism (Figure 5) include homolytic bond cleavages and the formation of Co^{II} or Co^{IV} as (transient) intermediates, as previously reported for $[Co_4O_4]$ at a lower level of theory (restricted to pure COSMO).[53] The new results with DCOSMO-RS additionally include an oxidative path that had been not explored and an extensive consideration of the spin states Table 3.

After addition of ROOH to $[Co_4O_4]$ (C1), intermediate **7-in** can follow two competing routes: (I) Oxidation of Co^{III} to Co^{IV} or (II) reduction of Co^{III} to Co^{II}. Along the oxidative route (I), **7-in** undergoes O−O bond dissociation (C2b-i) to form the (formal) Co^{IV} species **8-OH**, as mentioned above. Next, **8-OH** can abstract an H atom from another ROOH molecule, yielding **14** and ROO•. Finally, the catalyst (**1**) is regenerated by elimination of H_2O (C9a) or **7-in** by substitution of H_2O against ROOH (C9b). In the competing reductive route (II), adduct **7-in** first undergoes proton transfer from the OH group of ROOH to a μ_3-O atom of the cubane core. Subsequent homolytic CoO bond cleavage reduces one Co(III) center to Co(II) and releases an ROO• radical. The electronic structure of intermediate **11** is assigned to $[Co^{II}Co^{III}_3O_4]^{3+}$ based on IBO analysis (cmp. Figures S20 and S21). We assume that **11** is initially formed in the doublet state (**11-D**), but can relax to the quartet ground state (**11-Q**) *via* ISC (C4) (cf. Figure S27). This opens two possible pathways, starting either in the doublet or in the quartet state. In both cases, a second ROOH molecule is added (C5a/C5b), followed by homolytic O−O bond cleavage (C6a/C6b), which reoxidizes Co^{II} to Co^{III} and releases an RO• radical. Along the high-spin path, a triplet species (**13-T**) is formed, which must relax to the singlet ground state (**13-S**) via a second ISC step (C7). Finally, a proton transfer in **13-S** (from the μ_3−OH to the RO^- ligand) yields **14** which eliminates H_2O and regenerates the catalyst (**1**), thereby closing the catalytic cycle.

Table 3. Reaction Energies (In kJ/mol) for the ROOH Activation via Haber-Weiss Decomposition (Steps According to Figure 5, Energies Plotted Figure 6)

Step	Description	H_2O_2	TBHP
C1	ROOH addition	−17.9	−2.0
C2b	**Oxidative Route**		
C2b-i	O−O dissociation, elim. of RO•	119.1	69.5
C2b-ii	HAT[a] from ROOH, elim. of ROO•	−66.5	−74.9
C9b	Subst. of H_2O against ROOH	−8.8	7.1
	Reductive Route		
C3	Co−O homolysis ($Co^{+III} \rightarrow Co^{+II}$)	79.6	44.7
C2a	Proton transfer	17.2	27.8
	High-spin (HS) Path		
C4	ISC (D → Q)	−52.2	−52.2
C5a	ROOH addition	−24.1	13.3
C6a	O−O dissociation ($Co^{+II} \rightarrow Co^{+III}$)	103.0	31.8
C7	ISC (T → S)	−24.9	−24.9
	Low-spin (LS) Path		
C5b	ROOH addition	−15.7	8.9
C6b	O−O dissociation ($Co^{+II} \rightarrow Co^{+III}$)	17.5	−40.9
C8	Proton transfer	−46.0	−46.0
C9a	Elimination of H_2O	9.1	9.1
C1−C9a	2 ROOH → RO• + ROO• + H_2O	43.8	1.7

[a]HAT: Hydrogen Atom Transfer.

Downloaded from pubs.acs.org/inocaj/article-pdf/doi/10.1021/acs.inorgchem.6c03033/6828356/acs.inorgchem.6c03033.pdf by RUHR UNIVERSITAET BOCHUM user on 03 September 2026

https://doi.org/10.1021/acs.inorgchem.6c03033
Inorg. Chem. XXXX, XXX, XXX−XXX

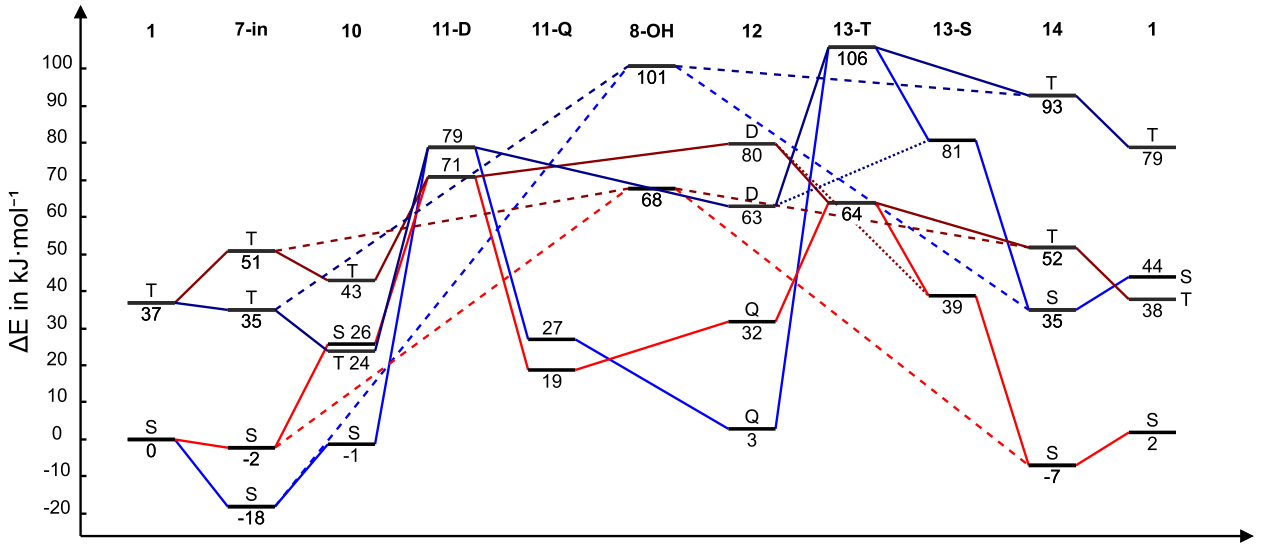


Figure 6. Energy diagram for the Haber-Weiss activation of H_2O_2 and TBHP for low-spin (LS) and high-spin (HS) paths (cf. Figure 5 and Table 3); Reductive pathways shown as full lines, oxidative pathways as dashed lines, for H_2O_2 as oxidant in blue (LS) and dark blue (HS) and for TBHP as oxidant in red (LS) and dark red (HS).

The energies for the different pathways are shown in Figure 6. The reductive high-spin pathways via **11-Q** (solid lines) exhibit two effective barriers based on the energy span: one associated with the first homolysis *via* steps C1−C3 (H_2O_2: ≈100 kJ/mol; TBHP: ≈80 kJ/mol), and a second associated with the O−O bond cleavage in step 6 (H_2O_2: ≈110 kJ/mol; TBHP: ≈45 kJ/mol). The low-spin pathway via **11-D** (dotted lines between **11-D**, **12-D**, and **13(S)**) substantially lowers the second barrier to approximately 10 kJ/mol for TBHP by bypassing the ISC steps. For H_2O_2, this effect is less pronounced, reducing the second barrier only to about 20−40 kJ/mol. The reason for this qualitative difference is that the elimination of HO• from the complex is endothermic while the elimination of RO• is exothermic. The oxidative pathway via **8-OH** (darker colors and dashed lines in Figure 6) exhibits a higher barrier (relative to the previous minimum) for H_2O_2 (ca. 120 kJ/mol) and is therefore unlikely to be relevant. For TBHP, however, the barrier (≈70 kJ/mol) is comparable to that of the reductive pathway (via **11**) and should be considered competitive. Overall, TBHP reveals the lowest energy span for the path via **8-OH**, closely followed by the paths via **12-D**/**13-S** and **12-Q**/**13-T**. For H_2O_2, the path via **12-D**/**13-S** is most feasible, followed by the paths via **8-OH** and **12-Q**/**13-T**.

Reactions starting from the triplet state of the catalyst **1** were also considered (Table S24 and Figure 6). The initial ISC from the singlet into the triplet state requires approximately 40 kJ/mol (with a vertical transition energy of ca. 75 kJ/mol). While the Haber-Weiss mechanism is certainly feasible starting from **1-T**, the reaction barriers remain unaltered, given that the same highest-lying intermediates (i.e., **11-D** and **8-OH**) are involved. Only if **1-T**, once formed, remains for several catalytic cycles in the triplet state and, thus, the ISC energy can be considered a one-time initial energetic cost, the total effective barriers are reduced: Both for the reductive route (H_2O_2: ∼ 45 kJ/mol; TBHP: ∼ 55 kJ/mol) and even more so for the oxidative route (H_2O_2: ∼ 75 kJ/mol; TBHP: ∼ 30 kJ/mol).

The Haber-Weiss mechanism describes a net decomposition of ROOH into RO• and ROO• according to

$$2\mathrm{ROOH} \rightarrow \mathrm{ROO}^{\bullet} + \mathrm{RO}^{\bullet} + \mathrm{H_2O} \quad (2)$$

with barriers that are significantly lower than those for direct dissociation of the peroxides into RO• and HO• radicals. Overall, the Haber-Weiss mechanism therefore represents the most plausible activation pathway. Furthermore, the results highlight differences between H_2O_2 and TBHP: the latter is more readily activated, as its conversion along the Haber-Weiss pathway does not require the formation of free HO• radicals and, thus, has an activation barrier that is ≈ 10 kJ/mol lower than for H_2O_2. According to the Arrhenius equation $\left(k = A\exp\left(-\frac{E_a}{RT}\right)\right)$, that difference in activation energy (E_a) translates into ratios of the corresponding rate constants (k) of ca. 60 at room temperature (25 °C) and ca. 30 at the experimental condition in ref 53. (82 °C), assuming identical pre-exponential factors (A) for H_2O_2 and TBHP.

This difference in ease of activation (or tendency of radical formation) between H_2O_2 and TBHP is in line with experimental observations (see refs [16,27] and those cited therein): (i) H_2O_2 typically requires slightly higher temperatures, leading to rapid self-decomposition (*vide infra*, cf. Table 4) and lower selectivity, whereas, TBHP performs oxidation at milder conditions, providing higher selectivities; (ii) When reacting with allylic alcohols, TBHP favors the formation of allylic oxidation products, while H_2O_2 favors epoxidation products.

Involvement of a Potential Co^V Species. Motivated by literature reports on the involvement of cobalt oxidation states higher than + III in alcohol oxidation with TBHP[29,32,48,49,91] and by the observations made above for O_2 activation, we investigated the potential involvement of a Co^V-oxo (Co^V=O) species[92] for the $[Co_4O_4]$ complex in the presence of TBHP. A possible path for the formation of a Co^V species on the triplet surface is shown in Figure 7(a). In a pathway deviating from the main Haber-Weiss mechanism, the adduct **7-in** could undergo a proton transfer to the second O atom in *t*-BuOOH, associated with a reaction energy of 51.5 kJ/mol. Elimination of *t*-BuOH (−26.1 kJ/mol) then yields species **16** in its triplet ground state, formally featuring a Co^V=O center. However,

Downloaded from pubs.acs.org/inocaj/article-pdf/doi/10.1021/acs.inorgchem.6c03033/6828356/acs.inorgchem.6c03033.pdf by RUHR UNIVERSITAET BOCHUM user on 03 September 2026

https://doi.org/10.1021/acs.inorgchem.6c03033
Inorg. Chem. XXXX, XXX, XXX−XXX

Table 4. Reaction Energies and Barriers (In kJ/mol) for Competing Radical Reactions

Reaction	Description	Energy[a]
	Reactions of RO• with HOOR	
1	$HO^{\bullet} + H_2O_2 \rightarrow H_2O + HOO^{\bullet}$	−141.7 (—)
2	$HO^{\bullet} + t\text{-}BuOOH \rightarrow H_2O + t\text{-}BuOO^{\bullet}$	−150.0 (—)
3	$tBuO^{\bullet} + t\text{-}BuOOH \rightarrow t\text{-}BuOH + t\text{-}BuOO^{\bullet}$	−92.5 (20.8)
	Reactions of RO• with ROO•	
4	$HO^{\bullet} + HOO^{\bullet} \rightarrow H_2O + O_2$	−261.1 (—)
5	$tBuO^{\bullet} + t\text{-}BuOO^{\bullet} \rightarrow t\text{-}Bu_2O + O_2$	−136.5 (≫ 100)[b]
	Reactions of ROO• with ROO•	
6	$HOO^{\bullet} + HOO^{\bullet} \rightarrow H_2O_2 + O_2$	−119.5 (3.8)

[a]Reaction barriers given in parentheses (if applicable). Barrierless (—). [b]Estimate based on a constraint geometry obtained from the optimized TS of the corresponding reaction with R = CH_3 and substitution of R with *t*-Bu.

intermediate **15** lies energetically approximately 25−30 kJ/mol above the highest intermediates along the Haber-Weiss pathways discussed above (**8-OH**, **12-D**, and **13-T**). On the singlet potential energy surface, the proton transfer step (C2c-i) is even more endothermic (115 kJ/mol), and no minimum could be located for intermediate **16**.

The electronic structure of **16-T** deserves special attention. It is best represented as a resonance hybrid between (**I**) O bound to Co^{III}, (**II**) O^- bound to Co^{IV}, and (**III**) O^{2-} bound to Co^{V}, as illustrated schematically in Figure 7(a). Similarly large spin densities at Co and O (Figure 7(b)) indicate a large weight of resonance structure **II** since the spin density would be exclusively localized at either O or Co^{V} in **I** and **III**, respectively. The IBOs (Figures S22−S23) suggest an interpretation of the bonding as a strongly polarized σ bond and half of a π bond between Co and O. Thus, a predominant Co^{IV}-oxyl (i.e., Co^{IV}−O) character, instead of a genuine Co^{V}-oxo (i.e., Co^{V}=O) is assigned to **16-T**. In fact, the bonding in **16** resembles that of a single Co−O pair in structure **4** obtained after O_2 dissociation at $[Co_4O_4]^{4+}$ (cf. Figure S1 and its discussion in the SI). This observation is consistent with the so-called oxo wall, which states that cobalt oxidation states above + III are generally unstable in an octahedral environment.[93,94]

Follow-Up Reactions. Once formed, the reactive RO• (i.e., HO• or *t*-BuO•) radicals can undergo follow-up reactions prior to alcohol oxidation (cf. Table 4). Most importantly, RO• can react exothermically and nearly barrierlessly with ROOH to form ROH and ROO• for both, R = H (rx. 1) and R = *t*-Bu (rx. 3). Due to their higher stability, the ROO• radicals, in particular *t*-BuOO•, are expected to have longer lifetimes, which is why they are considered the key species responsible for the alcohol oxidation. H_2O_2 is experimentally known to be an inactive oxidant for alcohol (*i*-PrOH, BnOH, CnOH) oxidations with $[Co_4O_4]$,[53] consistent with efficient recombination of HOO• with HO• or HOO• *via* a barrierless H atom transfer (HAT), leading to the formation of O_2 and H_2O (rx. 4) or H_2O_2 (rx. 6), respectively. In contrast, the analogous reactions between RO• and ROO• with R ≠ H (e.g., rx. 5) would involve attack at sp^3-hybridized carbon atoms with inversion, which is kinetically unfavorable for R = *t*-Bu due to a very high barrier associated with the steric demands of the *t*-Bu group. This explains the superior performance of TBHP compared to H_2O_2.

Alcohol Oxidation with O_2

Because of the high energetic costs associated with the formation of side-on bound superoxide **3** and the Co-oxyl intermediates **4** and **5**, we consider for the alcohol oxidation with O_2 only pathways in which O_2 is either weakly coordinated to $[Co_4O_4]$ or reacts as free O_2 with the alcohol.

Bound-Species Mechanisms. We begin with a mechanism in which both the alcohol (ROH) and the oxidant (O_2) coordinate to the catalyst (Figure 8, Table 5) with *i*-PrOH as a representative alcohol. As before, acetate (OAc) is chosen for ligand substitution. The first two steps involve the binding of *i*-PrOH (D1) and O_2 (D2a) via ligand substitution, accompanied by elimination of an OAc ligand. Together, these steps are strongly endothermic (ca. 120 kJ/mol). From this point, two pathways were identified:

- Proton-coupled electron transfer (PCET) from the alcoholic O−H to the O−O moiety (D3a), followed by a second PCET from the C_α−H bond (D4);
- Proton transfer from the alcohol OH to a cage oxygen atom (D3b), followed by PCET from the C_α−H bond in the coordinated alkoxide (D8), and a subsequent proton transfer. [A sub-branch of this route, where acetone is eliminated from **24** (competing with step D10a) is discussed in the SI (Figure S29 and Table S26).]

Along pathway (a), the first PCET (D3a) is significantly endothermic (126.3 kJ/mol), and associated with a higher barrier. In contrast, the initial proton transfer step (D3b) along pathway (b) is slightly endothermic (ca. 40 kJ/mol) and expected to be nearly barrierless due to solvent mediation in the protic environment. The subsequent PCET from the C_α−H bond (D8) is strongly exothermic (−113.2 kJ/mol) with a moderate barrier of ca. 50 kJ/mol.

The calculated barriers (Figure 9) do not indicate a clear preference between the O−H and deprotonation pathways for *i*-PrOH, based on barriers around 200 kJ/mol. In contrast, a clear preference for the deprotonation over the O−H pathway is seen for BnOH, with barriers of ca. 190 and 275 kJ/mol, respectively. The order of the subsequent product substitution steps (D5 and D6) does not significantly affect the kinetics of the alcohol oxidation. Note that a difference of 50 kJ/mol in

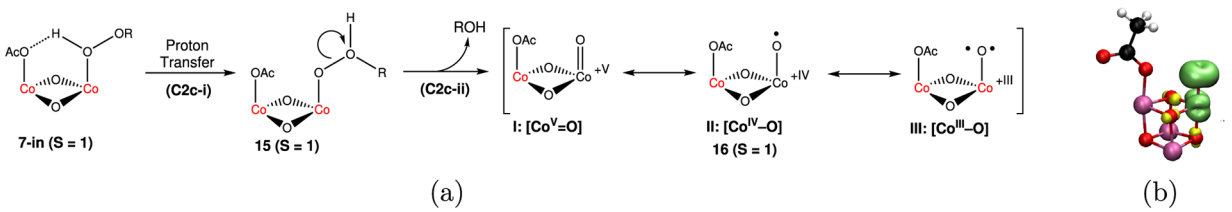


Figure 7. Formation with resonance structures (a) and spin density in the triplet ground state (b) of intermediate **16** involving higher oxidation states.

https://doi.org/10.1021/acs.inorgchem.6c03033
Inorg. Chem. XXXX, XXX, XXX−XXX

Downloaded from pubs.acs.org/inocaj/article-pdf/doi/10.1021/acs.inorgchem.6c03033/6828356/acs.inorgchem.6c03033.pdf by RUHR UNIVERSITAET BOCHUM user on 03 September 2026

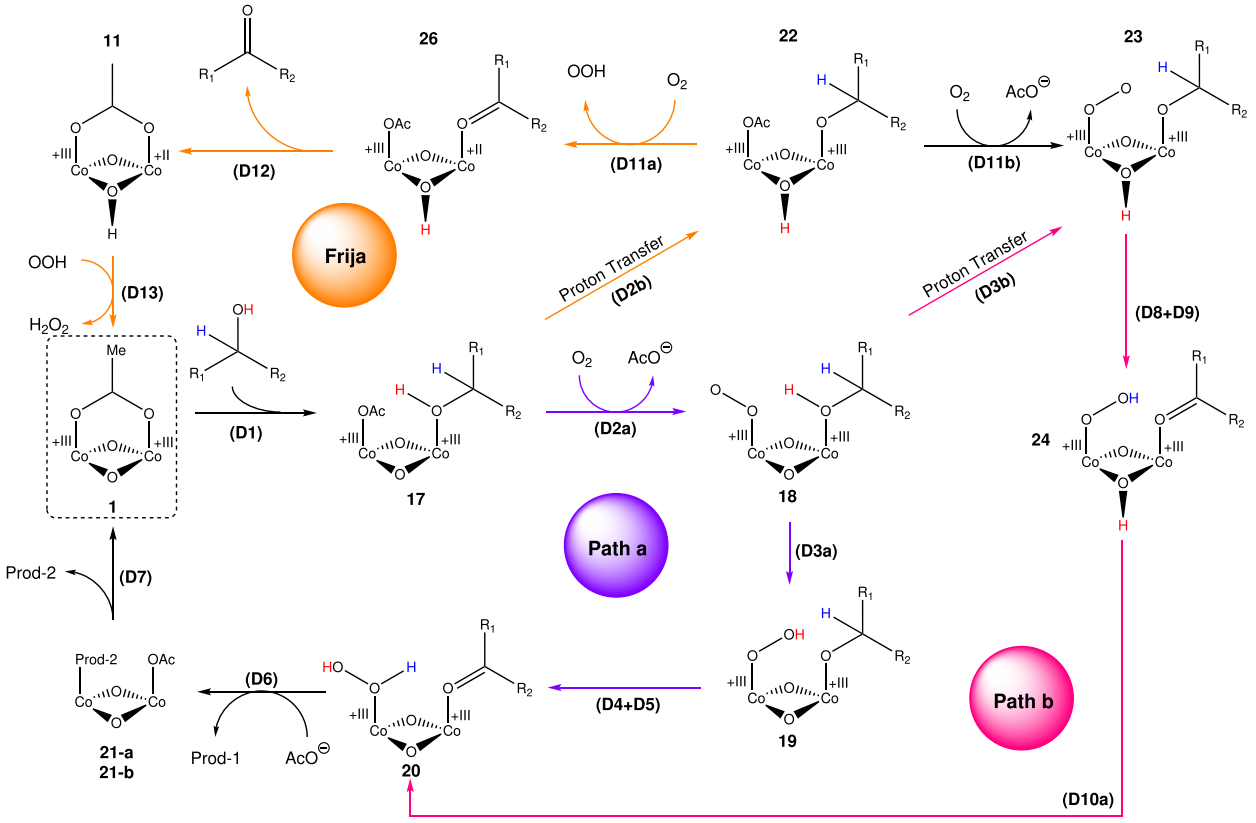


Figure 8. Mechanisms involving bound species and mixed bound-and-free species for the oxidation of *i*-PrOH ($R_1 = R_2 = CH_3$) and BnOH (R_1 = H, R_2 = Ph) and O_2 under formation of the ketone or aldehyde (energies and barriers given in Table 5); Colors: H atoms originating from the O–H (red) and C_α–H (blue); Path a (purple), b (pink) and Frija mechanism (orange).

Table 5. Reaction Energies and Barriers (In Parentheses) (In kJ/mol) for the Oxidation of *i*-PrOh with O_2 According to the Scheme Shown in Figure 8

Step	Description	*i*-PrOH	BnOH
D1	Alcohol (*i*-PrOH) addition	1.3	−8.3
D2a	Substitution of AcO^- against O_2	119.2	126.8
	O–H Pathway (a)		
D3a	PCET from O–H	36.5 (76.5)	113.7 (149.3)
D4	PCET from C_α–H	−79.5 (2.0)	−154.9 (34.0)
D5	ISC (T → S)	−91.7	−55.7
	Deprotonation Pathway (b)		
D3b	Deprotonation of OH and protonation of μ_3-O	39.8	34.2
D8	PCET from C_α–H	−152.5 (49.5)	−129.3 (34.4)
D9	ISC (T → S)	−30.0	−13.0
D10a	Deprotonation of μ_3–OH and protonation of ROO^-	8.0	11.2
D10b	Competing elimination of acetone under side-on binding of OOH	11.7	12.7
	Release of products		
D6	*Substitution of first product against AcO^-*		
D6a	Aldehyde/Ketone	−94.1	−119.9
D6b	H_2O_2	17.9	17.9
D7	*Substitution of second product against AcO^-*		
D7a	H_2O_2	−45.7	−83.0
D7b	Aldehyde/Ketone	−30.5	−19.0
	Mixed Bound-and-Free-Species (Frija) Mechanism		
D2b	Proton transfer in **17**	66.5	40.0
D11a	HAT from C_α–H by O_2	−61.3 (87.7)	−23.9 (67.1)
D12	Aldehyde/ketone elimination in **26**	−18.1 (22.4)	−9.4 (31.0)
D13	Reoxidation of **11** by $HOO^\bullet$ according to steps C4–C1	−78.9	−78.9
Total	$R^1R^2CHOH + O_2 \rightarrow R^1R^2CO + H_2O_2$	−90.4	−80.4

https://doi.org/10.1021/acs.inorgchem.6c03033
Inorg. Chem. XXXX, XXX, XXX−XXX

Downloaded from pubs.acs.org/inocaj/article-pdf/doi/10.1021/acs.inorgchem.6c03033/6828356/acs.inorgchem.6c03033.pdf by RUHR UNIVERSITAET BOCHUM user on 03 September 2026

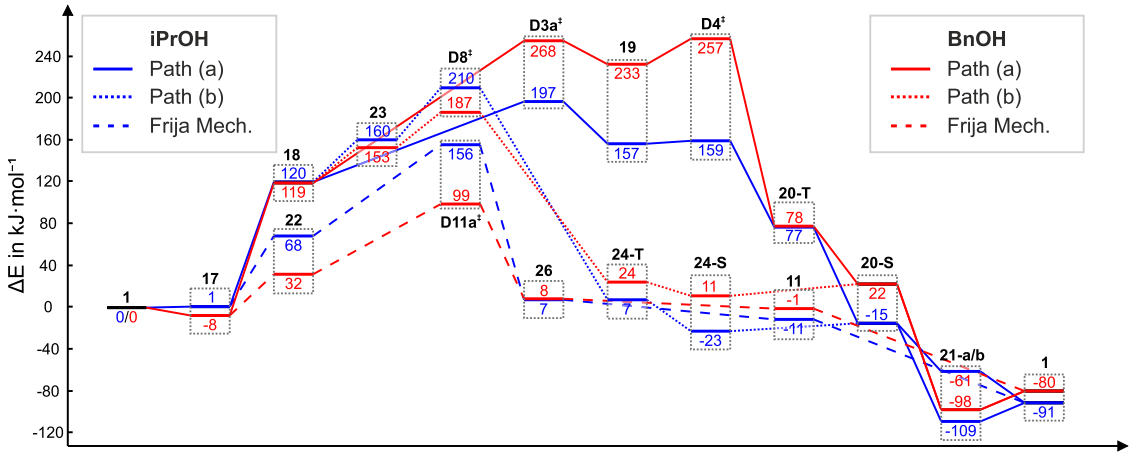


Figure 9. Energy diagram for the bound-species and mixed bound-and-free-species (Frija) reactions between *i*-PrOH (in blue) or BnOH (in red) and O_2 (cf. Figure 8 and Table 5).

activation energy corresponds to a rate constant ratio of ∼ 1.5 × 10^6 at 150 °C, i.e., the temperature for the experiments with O_2 in ref 53.

Mixed Bound-And-Free-Species (Frija) Mechanism. An alternative to the pathways described above, in which both O_2 and the alcohol are coordinated to $[Co_4O_4]$, is a mixed bound-and-free pathway, in which the alcohol is bound to the catalyst while O_2 reacts as a free species. This pathway is also included in Figure 9 and will be referred to as Frija mechanism in the following. It involves a proton transfer in adduct **17** (step D2b), followed by a PCET from the C_α–H bond to O_2, accompanied by reduction of one Co^{III} center to Co^{II} (D11a), similar to the Haber-Weiss mechanism. After product elimination (D12) from intermediate **26**, the reduced form of the catalyst **11** is reoxidized by HOO•. The energy profile indicates that this pathway is clearly preferred over mechanisms in which both reactants are coordinated to the catalyst: It exhibits significantly lower barriers of approximately 155 kJ/mol (*i*-PrOH) and 105 kJ/mol (BnOH). As for step D3b in the bound deprotonation pathway, the transition state for the HAT (step D11a) is 15–20 kJ/mol lower in energy for the more reactive BnOH compared to the less reactive *i*-PrOH.

Radical Chain Mechanism. Denisov and Denisova reported a radical chain mechanism involving the radicals $R^1R^2COH^•$, $R^1R^2C(OH)OO^•$, and $HOO^•$ as intermediates for liquid-phase alcohol oxidations with O_2.[95] Based on their work, a mechanism with the steps listed in Table 6 has been studied (see Table S27 for further details). A possible initiation step (I) could be the reaction of the alcohol with O_2, where via HAT from C_α–H would be preferred over HAT from O–H due to a less endothermic reaction energy and lower barrier. However, due to the high barrier, radicals that are more reactive are most likely needed to initiate the radical chains.

Anyway, in the subsequent propagation steps, O_2 and the O_2-derived $HOO^•$ radical are assumed to carry on the oxidation reaction. H abstraction from C_α–H of an alcohol by $HOO^•$ (P1) generates $R^1R^2COH^•$, slightly endothermic for *i*-PrOH and slightly exothermic for BnOH, with comparable barriers of ca. 40 kJ/mol. This hydroxyalkyl radical can react with O_2 (P2) to the ketone in a second exothermic and effectively barrierless HAT. In total, this mechanism also describes a net reduction of O_2 to H_2O_2.

Based on the mechanisms for alcohol oxidation with O_2 discussed so far, it can be summarized that the direct reactions between O_2 and the alcohols are associated with relatively high barriers, particularly for the initiation reactions. Here, we consider a barrier of 200 kJ/mol as a threshold for thermally accessible pathways with respect to the experimental conditions in ref 53. (150 °C, 10 bar). However, O_2 might react very well with $R^1R^2COH^•$ and could thus potentially support the oxidations with O_2 or ROOH. In particular, the barriers for the free-radical reactions are ca. 100 kJ/mol lower compared to both the bound and mixed bound-and-free mechanisms, resulting in a clear preference based on enormous ratios of the corresponding rate constants (∼ 2.2 × 10^{12}). Experimentally, such reactions between O_2 and organic radicals in alcohol oxidations have been postulated and kinetically modeled.[95−97] Other experimental studies on liquid-phase alcohol oxidations with O_2 typically involve harsher conditions (i.e., elevated temperature and pressure),[9,11] as it was also the case in ref 53. Moreover, for the related hydrocarbon oxidations, radical-chain reactions with O_2 are largely established.[13−16,20,50,51]

Table 6. Reaction Energies and Barriers (In kJ/mol) for the Alcohol Oxidations with O_2 Based on a Radical Chain Mechanism[a]

Step	Reaction	i-PrOH	BnOH
	Initiation		
I	$R^1R^2CHOH + O_2 \rightarrow R^1R^2COH^• + HOO^•$	143.6 (—)	98.3 (—)
	Propagation		
P1	$R^1R^2CHOH + HOO^• \rightarrow R^1R^2COH^• + HOOH$	24.2 (42.9)	−21.1 (38.7)
P2	$R^1R^2COH^• + O_2 \rightarrow R^1R^2CO + HOO^•$	−114.6 (—)	−59.3 (—)
	Termination		
T	$R^1R^2COH + HOO^• \rightarrow R^1R^2CO + HOOH$	−234.1 (—)	−178.7 (—)
P1+P2	$R^1R^2CHOH + O_2 \rightarrow R^1R^2CO + HOOH$	−90.4	−80.4

[a]Reaction barriers given in parentheses (if applicable). Barrierless reactions (—).

Alcohol Oxidation with ROOH

As discussed above, ROOH activation via the Haber-Weiss mechanism generates HOO• and ROO• as reactive species. In the following, $HOO^•$ and *t*-$BuOO^•$ are considered to be the radicals formed from H_2O_2 and TBHP, respectively. Results for

https://doi.org/10.1021/acs.inorgchem.6c03033
Inorg. Chem. XXXX, XXX, XXX−XXX

Downloaded from pubs.acs.org/inocaj/article-pdf/doi/10.1021/acs.inorgchem.6c03033/6828356/acs.inorgchem.6c03033.pdf by RUHR UNIVERSITAET BOCHUM user on 03 September 2026

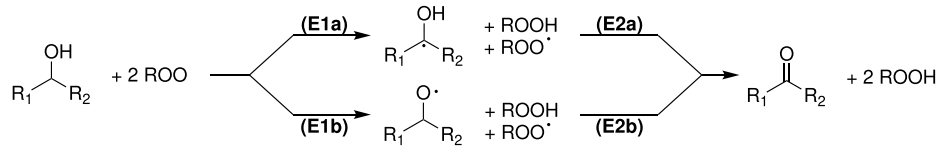


Figure 10. Free-radical reactions between a secondary alcohol and ROO• radicals under formation of the ketone (energies given in Table 7).

Table 7. Reaction Energies and Barriers for the Free-Radical Alcohol Oxidation Mechanism (Steps According to Figure 10)[a]

		i-PrOH		BnOH	
Step	Description	HOO•	*t*-BuOO•	HOO•	*t*-BuOO•
E1a	HAT from C_α–H	24.2 (42.9)	32.6 (51.5)	−17.6 (38.7)	−9.2 (46.0)
E1b	HAT from O–H	82.9 (79.3)[b]	91.3 (86.6)[b]	76.7 (72.2)[b]	85.1 (80.4)[b]
E2a	HAT from O–H	−234.1 (—)	−225.7 (—)	−178.7 (—)	−170.4 (—)
E2b	HAT from C_α–H	−292.8 (—)	−284.4 (—)	−272.6 (—)	−264.2 (—)

[a]Reaction barriers given in parentheses. Barrierless reactions (—). [b]Barrier for the reaction to a weakly bound complex of the products. The backward reaction from the separated products is effectively barrierless.

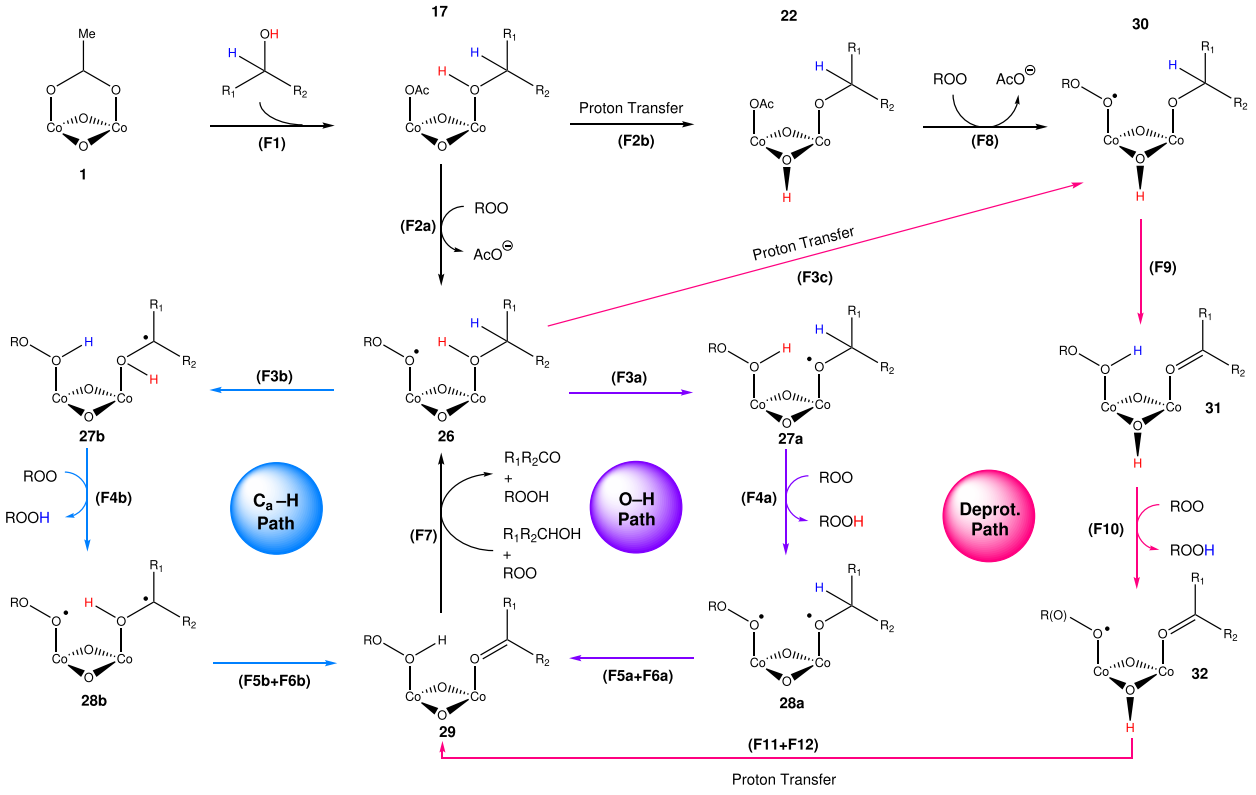


Figure 11. Bound-radical reactions between a primary or secondary alcohol (R^1R^2CHOH) and ROO• radicals under formation of the aldehyde or ketone with H atoms originating from the O–H in red and C_α–H in blue (energies and barriers given in Table 8); Pathway colors: O–H path (purple), C_α–H path (blue), and deprotonation path (pink). Substitution at the OAc ligand assumed; ISC steps F6a, F6b, and F11 are not explicitly shown.

the HO• radical, as an example of a highly reactive species, are given in the SI (Table S28). Analogous to the oxidation with O_2, we have investigated several possible mechanisms, differing in the binding of the reacting species and the sequence of PCET or HAT steps.

Free Radicals. First, we consider the simplest case, namely reactions between free species in solution that do not involve the $[Co_4O_4]$ complex (Figure 10). Two successive hydrogen atom transfer (HAT) steps at the alcohol (ROH), required to oxidize it to the corresponding ketone, are examined. Table 7 summarizes the reaction energies and barriers for the individual steps shown in Figure 10 for the alcohols *i*-PrOH and BnOH.

Hydrogen atom transfer from the C_α–H bond (step E1a) is favored, with activation barriers that are 30–40 kJ/mol lower than those for HAT from the O–H bond (step E1b). The second HAT is strongly exothermic for both the O–H (step E2a) and C_α–H (step E2b) pathways and effectively barrierless. The results highlight the different reactivity of the two oxidizing radicals:

https://doi.org/10.1021/acs.inorgchem.6c03033
Inorg. Chem. XXXX, XXX, XXX−XXX

Downloaded from pubs.acs.org/inocaj/article-pdf/doi/10.1021/acs.inorgchem.6c03033/6828356/acs.inorgchem.6c03033.pdf by RUHR UNIVERSITAET BOCHUM user on 03 September 2026

- For HOO•, the first HAT has activation barriers of approximately 50 and 80 kJ/mol for the C_α−H and the O−H bonds, respectively.
- *t*-BuOO• is less reactive than HOO• with both reaction energies and activation barriers that are approximately 10 kJ/mol higher.

Bound Radicals. An alternative to the above free-radical mechanism (Figure 10) is provided by bound-radical mechanisms, as summarized in Figure 11. Pathways which start with either cleavage of the O−H (a) or of the C_α−H (b) bond or with a proton transfer (c) from the alcoholic OH group to an oxygen atom of the $[Co_4O_4]$ cage are considered. Similar as with O_2 as oxidant, the C_α−H (and O−H) pathways involve the transient species **28b** (**28a**) that are no intermediates (i.e., minima on the PES), but undergo a second PCET directly Table 8.

Table 8. Reaction Energies and Barriers (In kJ/mol) for the Bound-Radical Reactions (Steps According to Figure 11)[a]

		i-PrOH		BnOH
Step	Description	HOO•	*t*-BuOO•	*t*-BuOO•
F1	Alcohol addition	1.3	1.3	−8.3
F2a	Substitution of AcO^- against oxidant	59.0	76.4	81.0
	O−H Pathway			
F3a	PCET from O−H	36.9 (44.5)	34.1 (31.7)	40.9 (56.8)
F4a	Substitution of ROOH against oxidant	34.9[b,c]	27.7[b,c]	5.3[b,c]
F5a	PCET from C_α−H	−174.0[b,c] (n.a.)	−201.1[b,c] (n.a.)	−153.0[b,c] (n.a.)
F6a	ISC	−91.7	−53.7	−83.2
	C_α−H Pathway			
F3b	PCET from C_α−H	66.6 (54.2)	59.6 (74.0)	22.0 (95.3)
F4b	Substitution of ROOH against oxidant	−89.3[b,d]	−105.3[b,d]	−14.6[b,d]
F5b	PCET from O−H	−79.5[b,d] (n.a.)	−93.6[b,d] (n.a.)	−114.3[b,d] (n.a.)
F6b	ISC	−91.7	−53.7	−78.9
	Deprotonation Pathway			
F3c	Deprotonation of OH and protonation of μ_3-O	39.4	31.0	18.5
F9	PCET from C_α−H	−147.4 (28.1)	−143.0 (8.6)	−71.9 (49.3)
F10	Substitution of R^1R^2CO against oxidant	−63.9	−41.8	−64.7
F11	ISC	−30.0	−20.4	−54.2
F12	Deprotonation of μ_3−OH and protonation of ROO^-	8.0	−18.8	−13.5
F7	Substitution of products against new reagents	−15.9	−0.2	2.6
3−5	$R^1R^2CHOH + 2\ ROO\bullet \rightarrow R^1R^2CO + 2\ ROOH$	−209.9	−193.2	−183.1

[a]Reaction barriers given in parentheses (if applicable). Barrierless reactions (—). Not available (n.a.). [b]Estimated based on constraint geometries. [c]Species **27a** unstable. [d]Species **27b** unstable.

The energy diagrams for the three different pathways are shown for *i*-PrOH/HOO•, *i*-PrOH/*t*-BuOO•, and BnOH/*t*-BuOO• in Figure 12. Step F3 is rate-determining for the C_α−H and O−H pathways with, respectively, **27** or **28** as the energetically highest intermediates, while step F9 leads to the highest intermediate **30** for the deprotonation pathway. Importantly, for *i*-PrOH, **30** (Figure 13(d)) is energetically more stable compared to **27a** (Figure 13(c)) or **27b** (Figure 13(b)) because the radical center is stabilized via interaction with a Co center, as visible in the spin densities (Figure 13). A similar interaction is possible in **27a**, but not in **27b**. After PCET in **30**, this stabilization even leads to an effective oxidation of the formal radical anion under reduction of Co^{III} to Co^{II} in **31** (Figure 13(e)).

The O−H pathways involve medium energy spans of 130−140 kJ/mol for all three combinations, whereas, the C_α−H pathways reveal a similar span of ca. 130 kJ/mol for *i*-PrOH/HOO•, but tend toward higher spans of 150−170 kJ/mol for *t*-BuOO•. In contrast, the deprotonation pathways tend toward lower spans of 140 kJ/mol for *i*-PrOH/HOO• and only ca. 110 kJ/mol for both alcohols with *t*-BuOO•. Additional comparisons for the alcohols and the oxidants are given in the SI (Sec. S10.2.2). Thus, the following pathways are identified as most favored:

- *i*-PrOH/HOO•: C_α−H pathway, closely followed by the deprotonation pathway
- *i*-PrOH/*t*-BuOO•: deprotonation pathway
- BnOH/*t*-BuOO•: O−H pathway.

Mixed Bound-And-Free Radical (Frija-Style) Mechanism. Motivated by the interactions observed for the O_2/alcohol systems and above between the $[Co_4O_4]$ cluster and the radicals formed from the alcohols after the first hydrogen abstraction, we investigated also for the oxidation with ROO• a mixed bound-free mechanism. The idea is that not both reactive species need to coordinate to $[Co_4O_4]$, thereby retaining a larger structural flexibility for the hydrogen transfer steps. This lead to the mechanism shown in Figure 14 (with the energies given in Table 9) which is similar to a mechanism described by Frija et al.for the oxidation of secondary alcohols with TBHP at mononuclear Cu^{II} and Co^{II} catalysts.[54,55]

In this mechanism, the alcohol is activated *via* addition to $[Co_4O_4]$ (step G1) and a proton transfer (PT) (step G2a) followed by a HAT from C_α−H to a ROO• radical (step G3a). Alternatively, the HAT (step G2b) can take place prior to the proton transfer (step G3b). Eventually, the alcohol is oxidized to the ketone, while one Co center is reduced from Co^{III} to Co^{II} (step G4). This step has been studied in the doublet state ($S = 1/2$) and the ISC into the quartet ($S = 3/2$) ground state as an optional subsequent step (see SI for further details). We focus on the doublet pathway since the spin does not affect the kinetics significantly, as these are downhill steps without additional barriers that occur after the rate-determing HAT (cf. Table S31). From intermediate **33**, the product can be eliminated, accompanied by an hapticity increase for OAc from η_1 to η_2 (step G4). Finally, the catalyst is reoxidized by another HAT to a ROO• radical.

The energies in Table 9 reflect that BnOH is more easily deprotonated than *i*-PrOH. For the pathway with PT before HAT, the proton transfer (G2a) is the only strongly endothermic step for both alcohols. On the doublet potential energy surface, reaction barriers of 15−30 kJ/mol for the HAT from C_α−H are found, which are ca. 20 kJ/mol lower than those for the free-radical reactions (Table 7). For the reaction route with a HAT (G2b) before the PT (G3b), the HAT is endothermic and has activation energies of ca. 50 and 60 kJ/mol for, respectively, HOO• and *t*-BuOO•. The subsequent proton transfer is largely exothermic and barrierless. Interestingly, intermediate **34** obtained in this step (G2b) has a spin density that is centered at the C atom and not at Co (Figure 15(a)), in difference to what would be expected for a

Downloaded from pubs.acs.org/inocaj/article-pdf/doi/10.1021/acs.inorgchem.6c03033/6828356/acs.inorgchem.6c03033.pdf by RUHR UNIVERSITAET BOCHUM user on 03 September 2026

https://doi.org/10.1021/acs.inorgchem.6c03033
Inorg. Chem. XXXX, XXX, XXX−XXX

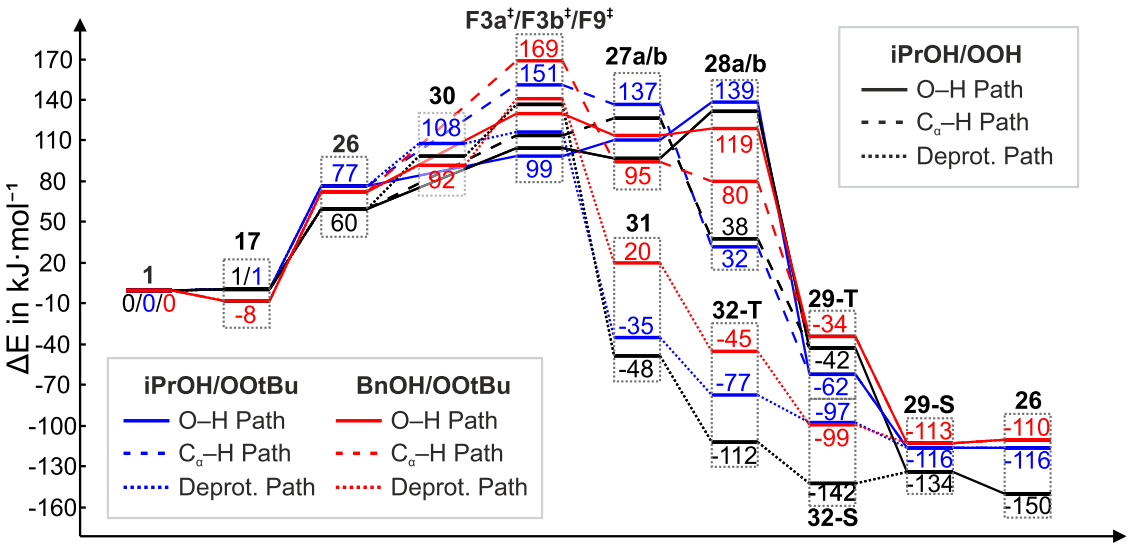


Figure 12. Energy diagram for the bound-radical reactions for the combinations *i*-PrOH/HOO• (black), *i*-PrOH/*t*-BuOO• (blue), and BnOH/*t*-BuOO• (red) (cf. Figure 11 and Table 8).

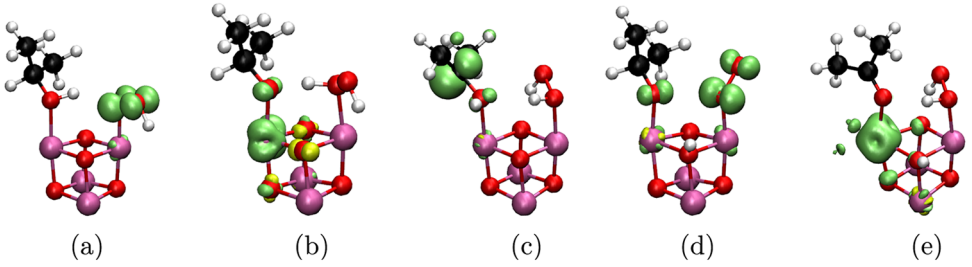


Figure 13. Spin densities of complexes with *i*-PrOH and HOO• differing in the order of the PCET and deprotonation: **26** (a), **27a** (b), **27b** (c) **30** (d), **31** (e).

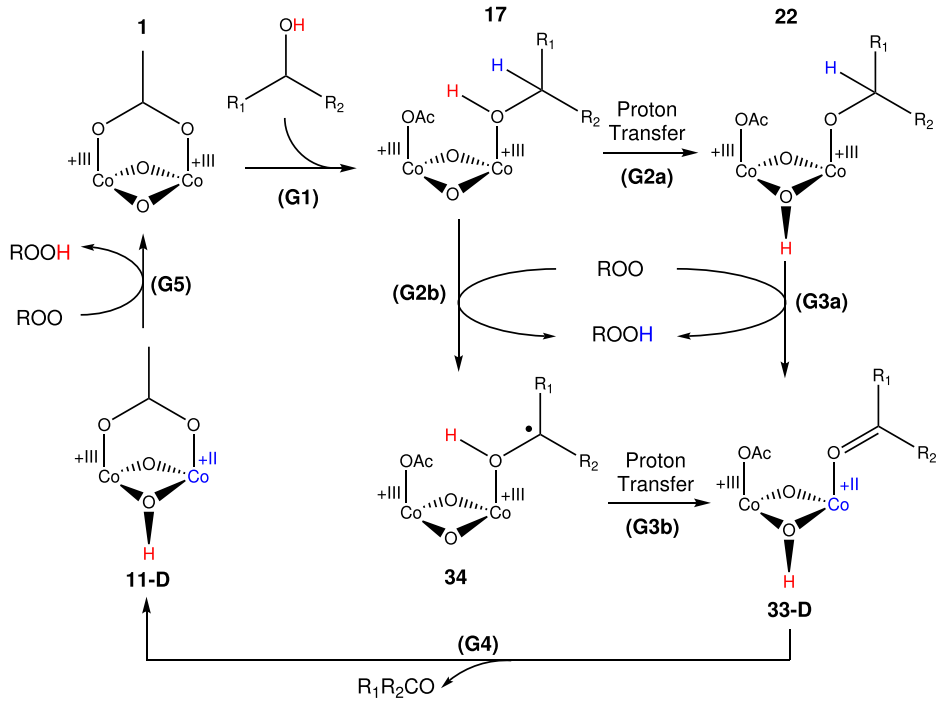


Figure 14. Frija-style mechanism for alcohol oxidation with H atoms originating from the O–H in red and C_α–H in blue (energies given in Table 9).

Downloaded from pubs.acs.org/inocaj/article-pdf/doi/10.1021/acs.inorgchem.6c03033/6828356/acs.inorgchem.6c03033.pdf by RUHR UNIVERSITAET BOCHUM user on 03 September 2026

https://doi.org/10.1021/acs.inorgchem.6c03033
Inorg. Chem. XXXX, XXX, XXX−XXX

Table 9. Energies and Barriers (In Parentheses) (In kJ/mol) for the Frija-Style Alcohol Oxidation Mechanism (Steps According to Figure 14)

		i-PrOH		BnOH	
Step	Description	HOO$^\bullet$	*t*-BuOO$^\bullet$	HOO$^\bullet$	*t*-BuOO$^\bullet$
G1	Alcohol addition	1.3	1.3	−8.3	−8.3
	Proton transfer before HAT				
G2a	Deprotonation of OH and protonation of μ_3-O	66.5	66.5	40.0	40.0
G3a	HAT from C_α−H by ROO$^\bullet$ while $Co^{+III} \rightarrow Co^{+II}$	−180.8 (25.9)	−172.4 (23.0)	−143.3 (15.2)	−135.0 (31.9)
	HAT before Proton transfer				
G2b	HAT from C_α−H by ROO$^\bullet$ while $Co^{+III} \rightarrow Co^{+II}$	20.9 (51.9)	29.3 (61.4)	−13.1 (50.5)	−4.8 (60.5)
G3b	Deprotonation of OH and protonation of μ_3-O	−135.2	−135.2	−90.2	−90.2
G4	Elimination of carbonyl under cage closing	−18.1	−18.1	−9.4	−9.4
G5	PCET	−78.9	−70.5	−78.9	−70.5

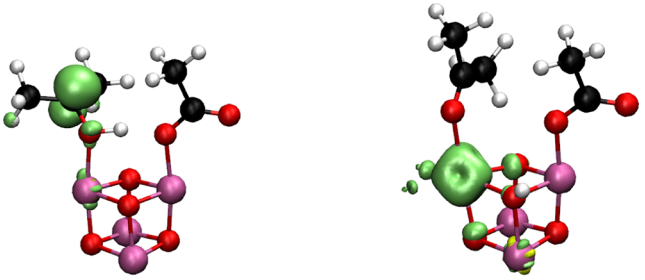


Figure 15. Spin densities of the complexes **34** and **33** involving PCETs prior to (a) or after PT (b), respectively.

protonated ketone. In contrast, the spin density is delocalized also over the Co if the proton transfer takes place before the PCET (Figure 15(b)).

The energy profiles for the four combinations of *i*-PrOH and BnOH with HOO$^\bullet$ and *t*-BuOO$^\bullet$ are shown in Figure 16. The first three steps, including the relevant transition states, are rate-determining because most subsequent steps are exothermic and barrierless. In the three cases except BnOH/*t*-BuOO$^\bullet$, the pathway with PCET before the proton transfer (G2b and G3b; blue) is found to be kinetically preferred over the pathway with PCET after a proton transfer (G2a and G3a; black). The difference in barriers is more pronounced for the more reactive HOO$^\bullet$ than for *t*-BuOO$^\bullet$ and for *i*-PrOH (HOO$^\bullet$: ≈40 kJ/mol; *t*-BuOO$^\bullet$: ∼ 30 kJ/mol) compared to BnOH (HOO$^\bullet$: ≈10 kJ/mol; *t*-BuOO$^\bullet$: ≈ − 5 kJ/mol). Also a third pathway has been considered, involving a second PCET instead of a PT after the first PCET (cf. Figure S31, Table S31), similar to the free and bound radical mechanisms discussed above. This pathway shares the effective barriers with the pathway where the PCET occurs before the PT, with the first PCET being rate-determining.

In summary, the mixed bound-and-free radical mechanisms appear similarly plausible as the free mechanisms, but hints toward the importance of activating the alcohol via deprotonation. Further evidence for this is given by free-radical mechanisms that involve an initial deprotonation, where deprotonation of the isolated alcohol is largely disfavored (see Sec. S10.4 in the SI for details). Yet, both free and mixed bound-and-free mechanisms appear more plausible than the mechanisms that involve binding of both the alcohol and the oxidant at the catalyst.

CONCLUSIONS

For $[Co_4O_4]$ complexes as catalysts and hydroperoxides (ROOH) as oxidants, the Haber-Weiss mechanism, which ultimately generates ROO$^\bullet$ radicals, is identified as the kinetically preferred pathway for oxidant activation. DFT calculations at the level of PBE0/def2-TZVP predict activation

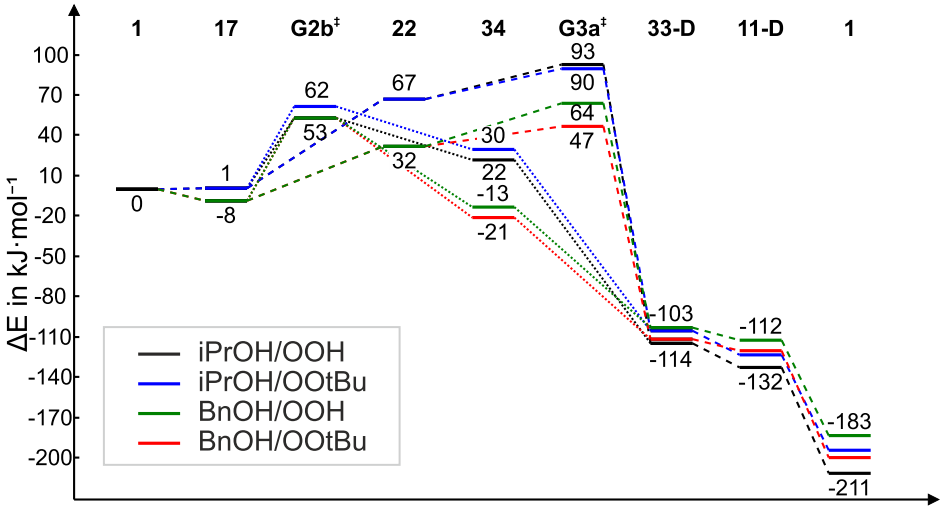


Figure 16. Energy diagrams for the Frija-style alcohol oxidations of *i*-PrOH and BnOH with HOO$^\bullet$ and *t*-BuOO$^\bullet$ following paths with either PT before (dashed lines) or after (dotted lines) HAT (cf. Figure 14 and Table 9).

https://doi.org/10.1021/acs.inorgchem.6c03033
Inorg. Chem. XXXX, XXX, XXX−XXX

Downloaded from pubs.acs.org/inocaj/article-pdf/doi/10.1021/acs.inorgchem.6c03033/6828356/acs.inorgchem.6c03033.pdf by RUHR UNIVERSITAET BOCHUM user on 03 September 2026

barriers of 80−90 kJ/mol for the activation of TBHP and approximately 120 kJ/mol for the activation of H_2O_2. Alternative reaction pathways involving cleavage of the RO−OH bond with formation of free HO• radicals are associated with significantly higher barriers due to the strong endothermic nature of these processes. The ROO• radicals act as the active oxidants in the alcohol oxidation, preferentially either in free-radical pathways or in catalytic cycles involving binding of the alcohol to the catalyst.

The finding that the most important pathways identified in the current work for $[Co_4O_4]$ under thermal conditions do not involve higher oxidation states differs from observations made under electrochemical conditions,[35] but appears to reflect the behavior of bulk cobalt oxide materials like spinels or perovskites.[20,50,51] In the Haber−Weiss mechanism, Co^{III} acts as an oxidant and Co^{II} as a reductant. Accordingly, the Co^{III}/Co^{II} redox cycle appears to be crucial, and lowering the barriers for the associated redox steps should facilitate ROOH activation further. An alternative Haber-Weiss pathway involving the oxidized catalyst, i.e., the Co^{III}/Co^{IV} redox pair, is also conceivable, but exhibits higher activation energies for the systems studied here. Stabilization of either the Co^{II} or the Co^{IV} intermediates may therefore provide a strategy to reduce these barriers and accelerate alcohol oxidation.

In contrast to ROOH, no significant O_2 activation is observed. While Gutiérrez-Tarriño et al. proposed dissociation into O adatoms or hydrogen abstraction for O_2 coordinated to Co_4O_4,[46] we find these processes to be highly endothermic and associated with high barriers. Therefore, we conclude that radical chain mechanisms are more likely operative in alcohol oxidation with O_2. Experimentally, it has been observed for catalyst **1** that O_2 can oxidize BnOH, but not *i*-PrOH.[53] This suggests a mechanism involving free radicals, which requires sufficiently stable alcohol-derived radical intermediates, consistent with the higher stability of benzyl compared to isopropyl radicals.

Opposing previous studies in the literature, we do not observe any competition between homolytic and heterolytic pathways (e.g., as reported by Lee et al. for olefin oxidation with peracids at $[Co_4O_4]$)[45] and no involvement of higher oxidation states (e.g., as reported for BnOH oxidation with TBHP at lower-nuclear complexes).[47−49] Instead, a clear preference for homolytic reactions is found for alcohol oxidations at $[Co_4O_4]$. In particular, a heterolytic mechanism involving a Co-oxo species and a concerted hydride shift, as reported by Thompson et al. for an immobilized hetero-bimetallic Co−Al complex, could not be identified.[49] Rather, the lowest barriers for alcohol oxidation at $[Co_4O_4]$ are found for a mechanism that closely resembles a mechanism proposed by Frija et al. for alcohol oxidation with TBHP at Co^{II} and Cu^{II} complexes.[54,55] This preference is supported by the experimental results reported in ref 53. from EPR spectroscopy for the oxidation of BnOH with TBHP catalyzed by $[Co_4O_4]$ which indicate that (i) Co^{II} is the only spin-active Co species, (ii) alkyl peroxyl (ROO•) is the dominant radical species, and (iii) alkyl oxyl (RO•) or other radicals are present only in trace amounts. These observations argue against the involvement of higher oxidation states of Co, which would be the case for the bound-radical mechanisms (involving Co^{IV}), or the active participation of alcohol-derived radicals (R^1R^2CHO or R^1R^2COH) in free solution, as in the case of free-radical reactions. Importantly, we identify in this work Co alkyl peroxyl species as intermediates in the catalytic alcohol oxidation with $[Co_4O_4]$. The involvement of such species as central intermediates had only been postulated before, e.g., by Chakrabarty et al.[44] for oxidation catalysis at $[Co_4O_4]^{4+}$ or in the context of stoichiometric peroxide decomposition and alcohol oxidation.[98−100]

The current mechanistic study also elucidates alcohol oxidation with O_2, assessing the reasons for their difficult thermal accessibility. Moreover, insights into the electronic structure of the central intermediates reveal important factors that govern the success of the alcohol oxidation with $[Co_4O_4]$, rooting in stabilization effects: (1) For alcohol oxidation, $[Co_4O_4]$ provides stabilization for the alcohol-centered radicals obtained after the first PCET step; (2) For oxidant activation, $[Co_4O_4]$ provides stabilization for the highly reactive HO• radical. Thus, in both cases, the generation of high-energy species is avoided, which opens reaction channels that involve much lower kinetic barriers compared with the uncatalyzed reactions in free solution.

■ ASSOCIATED CONTENT

Supporting Information

The Supporting Information is available free of charge at https://pubs.acs.org/doi/10.1021/acs.inorgchem.6c03033.

Effect of DCOSMO-RS structures on the reaction energies; Intrinsic Bond Orbitals (IBOs) for various species; Supporting Information on the mechanisms and additional mechanisms (PDF)

■ AUTHOR INFORMATION

Corresponding Author

Niklas Sülzner − *Lehrstuhl für Theoretische Chemie, Ruhr-Universität Bochum, Bochum 44780, Germany;* orcid.org/0000-0002-8734-5807; Phone: +49 (0)234 32-24250; Email: niklas.suelzner@rub.de

Authors

Melanie Alexandra Cedeño Manrique − *Lehrstuhl für Theoretische Chemie, Ruhr-Universität Bochum, Bochum 44780, Germany; Institute of Chemical Research of Catalonia (ICIQ), Tarragona 43007, Spain*

Christof Hättig − *Lehrstuhl für Theoretische Chemie, Ruhr-Universität Bochum, Bochum 44780, Germany;* orcid.org/0000-0002-5752-2710

Complete contact information is available at: https://pubs.acs.org/10.1021/acs.inorgchem.6c03033

Notes

The authors declare no competing financial interest.

■ ACKNOWLEDGMENTS

We thank the Deutsche Forschungsgemeinschaft (DFG, German Research Foundation) for funding through project 388390466 within the Collaborative Research Center CRC/TRR 247 (subproject A05) and under Germany's Excellence Strategy−EXC 2033−390677874−RESOLV. M.A.C.M has received a scholarship within RESOLV's "Solvation Scholars Undergraduate Exchange" program.

■ REFERENCES

(1) Gavriilidis, A.; Constantinou, A.; Hellgardt, K.; Hii, K. K. M.; Hutchings, G. J.; Brett, G. L.; Kuhn, S.; Marsden, S. P. Aerobic

https://doi.org/10.1021/acs.inorgchem.6c03033
Inorg. Chem. XXXX, XXX, XXX−XXX

Downloaded from pubs.acs.org/inocaj/article-pdf/doi/10.1021/acs.inorgchem.6c03033/6828356/acs.inorgchem.6c03033.pdf by RUHR UNIVERSITAET BOCHUM user on 03 September 2026

oxidations in flow: opportunities for the fine chemicals and pharmaceuticals industries. *React. Chem. Eng.* **2016**, *1*, 595−612.
(2) Ciriminna, R.; Pandarus, V.; Béland, F.; Xu, Y.-J.; Pagliaro, M. Heterogeneously Catalyzed Alcohol Oxidation for the Fine Chemical Industry. *Org. Process Res. Dev.* **2015**, *19*, 1554−1558.
(3) Sheldon, R. A. Fundamentals of green chemistry: efficiency in reaction design. *Chem. Soc. Rev.* **2012**, *41*, 1437−1451.
(4) Parmeggiani, C.; Matassini, C.; Cardona, F. A step forward towards sustainable aerobic alcohol oxidation: new and revised catalysts based on transition metals on solid supports. *Green Chem.* **2017**, *19*, 2030−2050.
(5) Ortega, K. F.; Anke, S.; Salamon, S.; Özcan, F.; Heese, J.; Andronescu, C.; Landers, J.; Wende, H.; Schuhmann, W.; Muhler, M.; et al. Topotactic Synthesis of Porous Cobalt Ferrite Platelets from a Layered Double Hydroxide Precursor and Their Application in Oxidation Catalysis. *Chem. - Eur. J.* **2017**, *23*, 12443−12449.
(6) Anke, S.; Bendt, G.; Sinev, I.; Hajiyani, H.; Antoni, H.; Zegkinoglou, I.; Jeon, H.; Pentcheva, R.; Roldan Cuenya, B.; Schulz, S.; Muhler, M. Selective 2-Propanol Oxidation over Unsupported Co3O4 Spinel Nanoparticles: Mechanistic Insights into Aerobic Oxidation of Alcohols. *ACS Catal.* **2019**, *9*, 5974−5985.
(7) Anke, S.; Falk, T.; Bendt, G.; Sinev, I.; Hävecker, M.; Antoni, H.; Zegkinoglou, I.; Jeon, H.; Knop-Gericke, A.; Schlögl, R.; Roldan Cuenya, B.; Schulz, S.; Muhler, M. On the reversible deactivation of cobalt ferrite spinel nanoparticles applied in selective 2-propanol oxidation. *J. Catal.* **2020**, *382*, 57−68.
(8) Dreyer, M.; Cruz, D.; Hagemann, U.; Zeller, P.; Heidelmann, M.; Salamon, S.; Landers, J.; Rabe, A.; Ortega, K. F.; Najafishirtari, S.; et al. The Effect of Water on the 2-Propanol Oxidation Activity of Co-Substituted LaFe1−xCoxO3 Perovskites. *Chem. - Eur. J.* **2021**, *27*, 17127−17144.
(9) Falk, T.; Budiyanto, E.; Dreyer, M.; Pflieger, C.; Waffel, D.; Büker, J.; Weidenthaler, C.; Ortega, K. F.; Behrens, M.; Tüysüz, H.; Muhler, M.; Peng, B. Identification of Active Sites in the Catalytic Oxidation of 2-Propanol over Co1+xFe2−xO4 Spinel Oxides at Solid/Liquid and Solid/Gas Interfaces. *ChemCatChem* **2021**, *13*, 2942−2951.
(10) Waffel, D.; Alkan, B.; Fu, Q.; Chen, Y.-T.; Schmidt, S.; Schulz, C.; Wiggers, H.; Muhler, M.; Peng, B. Towards Mechanistic Understanding of Liquid-Phase Cinnamyl Alcohol Oxidation with tert-Butyl Hydroperoxide over Noble-Metal-Free LaCo1−xFexO3 Perovskites. *ChemPlusChem* **2019**, *84*, 1155−1163.
(11) Waffel, D.; Budiyanto, E.; Porske, T.; Büker, J.; Falk, T.; Fu, Q.; Schmidt, S.; Tüysüz, H.; Muhler, M.; Peng, B. Investigation of Synergistic Effects between Co and Fe in Co3-xFexO4 Spinel Catalysts for the Liquid-Phase Oxidation of Aromatic Alcohols and Styrene. *Mol. Catal.* **2020**, *498*, 111251.
(12) Büker, J.; Alkan, B.; Fu, Q.; Xia, W.; Schulwitz, J.; Waffel, D.; Falk, T.; Schulz, C.; Wiggers, H.; Muhler, M.; Peng, B. Selective cyclohexene oxidation with O2, H2O2 and tert-butyl hydroperoxide over spray-flame synthesized LaCo1−xFexO3 nanoparticles. *Catal. Sci. Technol.* **2020**, *10*, 5196−5206.
(13) Büker, J.; Alkan, B.; Chabbra, S.; Kochetov, N.; Falk, T.; Schnegg, A.; Schulz, C.; Wiggers, H.; Muhler, M.; Peng, B. Liquid-Phase Cyclohexene Oxidation with O2 over Spray-Flame-Synthesized La1−xSrxCoO3 Perovskite Nanoparticles. *Chem. - Eur. J.* **2021**, *27*, 16912−16923.
(14) Büker, J.; Peng, B. Mechanistic insights into liquid-phase autoxidation of cyclohexene in acetonitrile. *Mol. Catal.* **2022**, *525*, 112367.
(15) Büker, J.; Angel, S.; Salamon, S.; Landers, J.; Falk, T.; Wende, H.; Wiggers, H.; Schulz, C.; Muhler, M.; Peng, B. Structure−activity correlation in aerobic cyclohexene oxidation and peroxide decomposition over CoxFe3−xO4 spinel oxides. *Catal. Sci. Technol.* **2022**, *12*, 3594−3605.
(16) Büker, J.; Muhler, M.; Peng, B. Concepts of Heterogeneously Catalyzed Liquid-Phase Oxidation of Cyclohexene with tert-Butyl Hydroperoxide, Hydrogen Peroxide and Molecular Oxygen. *ChemCatChem* **2023**, *15*, No. e202201216.
(17) Najafishirtari, S.; Friedel Ortega, K.; Douthwaite, M.; Pattisson, S.; Hutchings, G. J.; Bondue, C. J.; Tschulik, K.; Waffel, D.; Peng, B.; Deitermann, M.; et al. A Perspective on Heterogeneous Catalysts for the Selective Oxidation of Alcohols. *Chem. - Eur. J.* **2021**, *27*, 16809−16833.
(18) Xie, X.; Shen, W. Morphology control of cobalt oxidenanocrystals for promoting their catalytic performance. *Nanoscale* **2009**, *1*, 50−60.
(19) Li, Y.; Chen, T.; Zhao, S.; Wu, P.; Chong, Y.; Li, A.; Zhao, Y.; Chen, G.; Jin, X.; Qiu, Y.; Ye, D. Engineering Cobalt Oxide with Coexisting Cobalt Defects and Oxygen Vacancies for Enhanced Catalytic Oxidation of Toluene. *ACS Catal.* **2022**, *12*, 4906−4917.
(20) Hareendran, A.; Sato, T.; Dreyer, M.; Rabe, A.; Salamon, S.; Sülzner, N.; Hagemann, U.; Leiva-Leroy, C.; Cosanne, N.; Ravi, K.; Zhang, D.; Busser, G. W.; Behrens, M.; Hättig, C.; Wende, H.; Schnegg, A.; Muhler, M. Mechanistic and Structural Insights into the Liquid-Phase Oxidation of Cyclohexane over LaCo0.7Fe0.3O3 Perovskite Nanoparticles. *ACS Catal.* **2025**, *15*, 12773−12789.
(21) Nemati Kharat, A.; Bakhoda, A.; Tamaddoni Jahromi, B. Green and chemoselective oxidation of alcohols with hydrogen peroxide: A comparative study on Co(II) and Co(III) activity toward oxidation of alcohols. *Polyhedron* **2011**, *30*, 2768−2775.
(22) Barton, D. H. R.; Gloahec, V. N. L.; Patin, H.; Launay, F. Radical chemistry of tert-butyl hydroperoxide (TBHP). Part 1. Studies of the FeIII−TBHP mechanism. *New J. Chem.* **1998**, *22*, 559−563.
(23) Barton, D. H. R.; Gloahec, V. N. L.; Patin, H. Radical chemistry of tert-butyl hydroperoxide (TBHP). Part 2. Studies of the FeII−TBHP mechanism. *New J. Chem.* **1998**, *22*, 565−568.
(24) Turrá, N.; Neuenschwander, U.; Baiker, A.; Peeters, J.; Hermans, I. Mechanism of the Catalytic Deperoxidation of tert-Butylhydroperoxide with Cobalt(II) Acetylacetonate. *Chem. - Eur. J.* **2010**, *16*, 13226−13235.
(25) Willms, T.; Kryk, H.; Oertel, J.; Lu, X.; Hampel, U. Reactivity of t-butyl hydroperoxide and t-butyl peroxide toward reactor materials measured by a microcalorimetric method at 30 °C. *J. Therm. Anal. Calorim.* **2017**, *128*, 319−333.
(26) Willms, T.; Kryk, H.; Oertel, J.; Hempel, C.; Knitt, F.; Hampel, U. On the thermal decomposition of tert.-butyl hydroperoxide, its sensitivity to metals and its kinetics, studied by thermoanalytic methods. *Thermochim. Acta* **2019**, *672*, 25−42.
(27) Büker, J.; Shang, J.; Angel, S.; Budiyanto, E.; Tüysüz, H.; Wiggers, H.; Schulz, C.; Grünewald, M.; Peng, B.; Muhler, M. Tert-butyl hydroperoxide decomposition as a descriptor for liquid-phase hydrocarbon oxidation over transition metal oxide-based catalysts: a screening study. *Arkivoc* **2024**, *2024*, 202312158.
(28) Dimitrou, K.; Folting, K.; Streib, W. E.; Christou, G. Dimerization of the [Co2III(OH)2] core to the first example of a [Co4IIIO4] cubane: potential insights into photosynthetic water oxidation. *J. Am. Chem. Soc.* **1993**, *115*, 6432−6433.
(29) Nguyen, A. I.; Ziegler, M. S.; Oña-Burgos, P.; Sturzbecher-Hohne, M.; Kim, W.; Bellone, D. E.; Tilley, T. D. Mechanistic Investigations of Water Oxidation by a Molecular Cobalt Oxide Analogue: Evidence for a Highly Oxidized Intermediate and Exclusive Terminal Oxo Participation. *J. Am. Chem. Soc.* **2015**, *137*, 12865−12872.
(30) Nguyen, A. I.; Wang, J.; Levine, D. S.; Ziegler, M. S.; Tilley, T. D. Synthetic control and empirical prediction of redox potentials for Co4O4 cubanes over a 1.4 V range: implications for catalyst design and evaluation of high-valent intermediates in water oxidation. *Chem. Sci.* **2017**, *8*, 4274−4284.
(31) Nguyen, A. I.; Van Allsburg, K. M.; Terban, M. W.; Bajdich, M.; Oktawiec, J.; Amtawong, J.; Ziegler, M. S.; Dombrowski, J. P.; Lakshmi, K. V.; Drisdell, W. S.; Yano, J.; Billinge, S. J. L.; Tilley, T. D. Stabilization of reactive Co4O4 cubane oxygen-evolution catalysts within porous frameworks. *Proc. Natl. Acad. Sci. U. S. A.* **2019**, *116*, 11630−11639.
(32) McAlpin, J. G.; Stich, T. A.; Ohlin, C. A.; Surendranath, Y.; Nocera, D. G.; Casey, W. H.; Britt, R. D. Electronic Structure

Downloaded from pubs.acs.org/inocaj/article-pdf/doi/10.1021/acs.inorgchem.6c03033/6828356/acs.inorgchem.6c03033.pdf by RUHR UNIVERSITAET BOCHUM user on 03 September 2026

https://doi.org/10.1021/acs.inorgchem.6c03033
Inorg. Chem. XXXX, XXX, XXX−XXX

Description of a [Co(III)3Co(IV)O4] Cluster: A Model for the Paramagnetic Intermediate in Cobalt-Catalyzed Water Oxidation. *J. Am. Chem. Soc.* **2011**, *133*, 15444−15452.
(33) Hadt, R. G.; Hayes, D.; Brodsky, C. N.; Ullman, A. M.; Casa, D. M.; Upton, M. H.; Nocera, D. G.; Chen, L. X. X-ray Spectroscopic Characterization of Co(IV) and Metal−Metal Interactions in Co4O4: Electronic Structure Contributions to the Formation of High-Valent States Relevant to the Oxygen Evolution Reaction. *J. Am. Chem. Soc.* **2016**, *138*, 11017−11030.
(34) Brodsky, C. N.; Hadt, R. G.; Hayes, D.; Reinhart, B. J.; Li, N.; Chen, L. X.; Nocera, D. G. In situ characterization of cofacial Co(IV) centers in Co4O4 cubane: Modeling the high-valent active site in oxygen-evolving catalysts. *Proc. Natl. Acad. Sci. U. S. A.* **2017**, *114*, 3855−3860.
(35) Amtawong, J.; Nguyen, A. I.; Tilley, T. D. Mechanistic Aspects of Cobalt−Oxo Cubane Clusters in Oxidation Chemistry. *J. Am. Chem. Soc.* **2022**, *144*, 1475−1492.
(36) Beattie, J. K.; Hambley, T. W.; Klepetko, J. A.; Masters, A. F.; Turner, P. The chemistry of cobalt acetate-IV. The isolation and crystal structure of the symmetric cubane, tetrakis[(μ-acetato)(μ3-oxo) (pyridine)cobalt(III)] · chloroform solvate, [Co4(μ3-O)4(μ-CH3CO2)4(C5H5N) *in*4] · 5CHCl3 and of the dicationic partial cubane, trimeric, [(μ-acetato)(acetato)tris(μ-hdyroxy(μ3-oxo) hexakispyridinetricobalt(III)]hexafluorophosphate · water solvate, [Co3(μ3-O)(μ-OH)3(μ-CH3CO2(CH3CO2(C5H5N)6[PF6]2 · 2H2O. *Polyhedron* **1998**, *17*, 1343−1354.
(37) Chakrabarty, R.; Das, B. K. Epoxidation of α-pinene catalysed by tetrameric cobalt(III) complexes. *J. Mol. Catal. A: Chem.* **2004**, *223*, 39−44.
(38) Chakrabarty, R.; Bora, S. J.; Das, B. K. Synthesis, Structure, Spectral and Electrochemical Properties, and Catalytic Use of Cobalt(III)−Oxo Cubane Clusters. *Inorg. Chem.* **2007**, *46*, 9450−9462.
(39) Chakrabarty, R.; Das, B. K.; Clark, J. H. Enhanced selectivity in green catalytic epoxidation using a supported cobalt complex. *Green Chem.* **2007**, *9*, 845−848.
(40) Das, B. K.; Chakrabarty, R. Cobalt(III)-oxo cubane clusters as catalysts for oxidation of organic substrates. *J. Chem. Sci.* **2011**, *123*, 163−173.
(41) Sarmah, P.; Das, B. K. Catalysis of TBHP oxidation of styrene and diphenylmethane by a supported cobalt(III)-oxo cluster. *Indian J. Chem. Sect. A* **2014**, *53*, 41−45.
(42) Chakrabarty, R.; Kalita, D.; Das, B. K. Catalytic oxidation of *p*-xylene in water by cobalt(III) cubane cluster. *Polyhedron* **2007**, *26*, 1239−1244.
(43) Sarmah, P.; Chakrabarty, R.; Phukan, P.; Das, B. K. Selective oxidation of alcohols catalysed by a cubane-like Co(III) oxo cluster immobilised on porous organomodified silica. *J. Mol. Catal. A: Chem.* **2007**, *268*, 36−44.
(44) Chakrabarty, R.; Sarmah, P.; Saha, B.; Chakravorty, S.; Das, B. K. Catalytic Properties of Cobalt(III)−Oxo Cubanes in the TBHP Oxidation of Benzylic Alcohols. *Inorg. Chem.* **2009**, *48*, 6371−6379.
(45) Lee, S. Y.; Kim, N.; Lee, M. M.; Jo, Y. D.; Bae, J. M.; Hyun, M. Y.; Yoon, S.; Kim, C. A discrete Co4(μ3-OH)44+ cluster with an oxygen-rich coordination environment as a catalyst for the epoxidation of various olefins. *Dalton Trans.* **2016**, *45*, 1727−1736.
(46) Gutiérrez-Tarriño, S.; Gaona-Miguélez, J.; Oña-Burgos, P. Tailoring the electron density of cobalt oxide clusters to provide highly selective superoxide and peroxide species for aerobic cyclohexane oxidation. *Dalton Trans.* **2021**, *50*, 15370−15379.
(47) Boitsov, S.; Songstad, J.; Muzart, J. Chromium(vi) oxide− tert -butyl hydroperoxide interactions: evidence for a tert -butylperoxychromium complex and its role in the catalytic oxidation of alcohols. *J. Chem. Soc., Perkin Trans. 2* **2001**, *30*, 2318−2323.
(48) Rothenberg, G.; Feldberg, L.; Wiener, H.; Sasson, Y. Copper-catalyzed homolytic and heterolytic benzylic and allylic oxidation using tert -butyl hydroperoxide. *J. Chem. Soc., Perkin Trans. 2* **1998**, *27*, 2429−2434.
(49) Thompson, A. B.; Pahls, D. R.; Bernales, V.; Gallington, L. C.; Malonzo, C. D.; Webber, T.; Tereniak, S. J.; Wang, T. C.; Desai, S. P.; Li, Z.; Kim, I. S.; Gagliardi, L.; Penn, R. L.; Chapman, K. W.; Stein, A.; Farha, O. K.; Hupp, J. T.; Martinson, A. B. F.; Lu, C. C. Installing Heterobimetallic Cobalt−Aluminum Single Sites on a Metal Organic Framework Support. *Chem. Mater.* **2016**, *28*, 6753−6762.
(50) Hareendran, A.; Dreyer, M.; Sato, T.; Cosanne, N.; Leroy, C. L.; Peng, B.; Behrens, M.; Schnegg, A.; Muhler, M. Aerobic Oxidation of Cyclohexane over LaCoxFe1-xO3 Perovskites in the Liquid Phase. *Mol. Catal.* **2024**, *569*, 114615.
(51) Hareendran, A.; Sato, T.; Müller, L.; Rabe, A.; Ravi, K.; Zhang, D.; Busser, G. W.; Leiva-Leroy, C.; Wende, H.; Wiggers, H.; Schulz, C.; Schnegg, A.; Muhler, M. Aerobic Cyclohexane Oxidation Catalyzed by Vanadium-Substituted LaCoO3 Perovskites in the Liquid Phase. *ChemCatChem* **2026**, *18*, e01190.
(52) Fockenberg, T.; Sülzner, N.; Amin, H. M. A.; Wölper, C.; Hättig, C.; Schulz, S. Synthesis, Characterization, and Electrochemical Properties of Tri- and Tetranuclear CoIII-Oxo Complexes. *Eur. J. Inorg. Chem.* **2025**, *28*, e202500170.
(53) Fockenberg, T.; Sülzner, N.; Sato, T.; Zhang, D.; Hareendran, A.; Reher, J. M.; Tewes, J.; Schnegg, A.; Muhler, M.; Hättig, C.; et al. Comparative Study on the Catalytic Activity of [CoIII4O4] Heterocubanes in Alcohol Oxidation Reactions in Solution. *ACS Catal.* **2026**, *16*, 6355−6367.
(54) Frija, L. M. T.; Alegria, E. C. B. A.; Sutradhar, M.; Cristiano, M. L. S.; Ismael, A.; Kopylovich, M. N.; Pombeiro, A. J. L. Copper(II) and cobalt(II) tetrazole-saccharinate complexes as effective catalysts for oxidation of secondary alcohols. *J. Mol. Catal. A: Chem.* **2016**, *425*, 283−290.
(55) Frija, L. M. T. A convenient TBHP/Cu(NO3)2·2.5H2O-mediated oxidation of secondary and benzyl alcohols under microwave irradiation. *J. Chem. Sci.* **2025**, *137*, 60.
(56) *TURBOMOLE V7.9 2024, a development of University of Karlsruhe and Forschungszentrum Karlsruhe GmbH, 1989−2007*; 2024, TURBOMOLE GmbH. https://www.turbomole.org.
(57) Franzke, Y. J.; Holzer, C.; Andersen, J. H.; Begušić, T.; Bruder, F.; Coriani, S.; Della Sala, F.; Fabiano, E.; Fedotov, D. A.; Fürst, S.; Gillhuber, S.; Grotjahn, R.; Kaupp, M.; Kehry, M.; Krstić, M.; Mack, F.; Majumdar, S.; Nguyen, B. D.; Parker, S. M.; Pauly, F.; Pausch, A.; Perlt, E.; Phun, G. S.; Rajabi, A.; Rappoport, D.; Samal, B.; Schrader, T.; Sharma, M.; Tapavicza, E.; Treß, R. S.; Voora, V.; Wodyński, A.; Yu, J. M.; Zerulla, B.; Furche, F.; Hättig, C.; Sierka, M.; Tew, D. P.; Weigend, F. TURBOMOLE: Today and Tomorrow. *J. Chem. Theory Comput.* **2023**, *19*, 6859−6890.
(58) Eichkorn, K.; Treutler, O.; Öhm, H.; Häser, M.; Ahlrichs, R. Auxiliary basis sets to approximate Coulomb potentials. *Chem. Phys. Lett.* **1995**, *242*, 652−660.
(59) Treutler, O.; Ahlrichs, R. Efficient molecular numerical integration schemes. *J. Chem. Phys.* **1995**, *102*, 346−354.
(60) Eichkorn, K.; Weigend, F.; Treutler, O.; Ahlrichs, R. Auxiliary basis sets for main row atoms and transition metals and their use to approximate Coulomb potentials. *Theor. Chem. Acc.* **1997**, *97*, 119−124.
(61) Perdew, J. P.; Wang, Y. Accurate and simple analytic representation of the electron-gas correlation energy. *Phys. Rev. B* **1992**, *45*, 13244−13249.
(62) Perdew, J. P.; Burke, K.; Ernzerhof, M. Generalized Gradient Approximation Made Simple. *Phys. Rev. Lett.* **1996**, *77*, 3865−3868.
(63) Perdew, J. P.; Ernzerhof, M.; Burke, K. Rationale for mixing exact exchange with density functional approximations. *J. Chem. Phys.* **1996**, *105*, 9982−9985.
(64) Weigend, F.; Ahlrichs, R. Balanced basis sets of split valence, triple zeta valence and quadruple zeta valence quality for H to Rn: Design and assessment of accuracy. *Phys. Chem. Chem. Phys.* **2005**, *7*, 3297−3305.
(65) Schäfer, A.; Klamt, A.; Sattel, D.; Lohrenz, J. C. W.; Eckert, F. COSMO Implementation in TURBOMOLE: Extension of an efficient quantum chemical code towards liquid systems. *Phys. Chem. Chem. Phys.* **2000**, *2*, 2187−2193.

Downloaded from pubs.acs.org/inocaj/article-pdf/doi/10.1021/acs.inorgchem.6c03033/6828356/acs.inorgchem.6c03033.pdf by RUHR UNIVERSITAET BOCHUM user on 03 September 2026

(66) Klamt, A. The COSMO and COSMO-RS solvation models. *WIREs Comput. Mol. Sci.* **2018**, *8*, e1338.
(67) Pausch, A. Consistent Analytical Second Derivatives of the Kohn−Sham DFT Energy in the Framework of the Conductor-Like Screening Model through Gaussian Charge Distributions. *J. Chem. Theory Comput.* **2024**, *20*, 3169−3183.
(68) Høst, S.; Olsen, J.; Jansík, B.; Thøgersen, L.; Jørgensen, P.; Helgaker, T. The augmented Roothaan−Hall method for optimizing Hartree−Fock and Kohn−Sham density matrices. *J. Chem. Phys.* **2008**, *129*, 124106.
(69) Sülzner, N.; Hättig, C. Raw Data to "Mechanisms of Alcohol Oxidation Catalyzed by Co(III)-Oxo Cubanes: A Computational Study" *Zenodo*, 2026.
(70) Angnes, R. A. *mechaSVG*; 2020, GitHub repository.
(71) Knizia, G. Intrinsic Atomic Orbitals: An Unbiased Bridge between Quantum Theory and Chemical Concepts. *J. Chem. Theory Comput.* **2013**, *9*, 4834−4843.
(72) Deglmann, P.; May, K.; Furche, F.; Ahlrichs, R. Nuclear second analytical derivative calculations using auxiliary basis set expansions. *Chem. Phys. Lett.* **2004**, *384*, 103−107.
(73) Sinnecker, S.; Rajendran, A.; Klamt, A.; Diedenhofen, M.; Neese, F. Calculation of Solvent Shifts on Electronic g-Tensors with the Conductor-Like Screening Model (COSMO) and Its Self-Consistent Generalization to Real Solvents (Direct COSMO-RS). *J. Phys. Chem. A* **2006**, *110*, 2235−2245.
(74) Klamt, A.; Diedenhofen, M. Calculation of Solvation Free Energies with DCOSMO-RS. *J. Phys. Chem. A* **2015**, *119*, 5439−5445.
(75) Klamt, A.; Jonas, V.; Bürger, T.; Lohrenz, J. C. W. Refinement and Parametrization of COSMO-RS. *J. Phys. Chem. A* **1998**, *102*, 5074−5085.
(76) *BIOVIA COSMOtherm*; 2021, Dassault Systèmes. http://www.3ds.com.
(77) Vydrov, O. A.; Scuseria, G. E. Assessment of a long-range corrected hybrid functional. *J. Chem. Phys.* **2006**, *125*, 234109.
(78) McCool, N. S.; Robinson, D. M.; Sheats, J. E.; Dismukes, G. C. A Co4O4 "Cubane" Water Oxidation Catalyst Inspired by Photosynthesis. *J. Am. Chem. Soc.* **2011**, *133*, 11446−11449.
(79) Evangelisti, F.; Güttinger, R.; Moré, R.; Luber, S.; Patzke, G. R. Closer to Photosystem II: A Co4O4 Cubane Catalyst with Flexible Ligand Architecture. *J. Am. Chem. Soc.* **2013**, *135*, 18734−18737.
(80) Li, X.; Siegbahn, P. E. M. Water Oxidation Mechanism for Synthetic Co−Oxides with Small Nuclearity. *J. Am. Chem. Soc.* **2013**, *135*, 13804−13813.
(81) Smith, P. F.; Kaplan, C.; Sheats, J. E.; Robinson, D. M.; McCool, N. S.; Mezle, N.; Dismukes, G. C. What Determines Catalyst Functionality in Molecular Water Oxidation? Dependence on Ligands and Metal Nuclearity in Cobalt Clusters. *Inorg. Chem.* **2014**, *53*, 2113−2121.
(82) Li, X.; Clatworthy, E. B.; Masters, A. F.; Maschmeyer, T. Molecular Cobalt Clusters as Precursors of Distinct Active Species in Electrochemical, Photochemical, and Photoelectrochemical Water Oxidation Reactions in Phosphate Electrolytes. *Chem. - Eur. J.* **2015**, *21*, 16578−16584.
(83) Hodel, F. H.; Luber, S. What Influences the Water Oxidation Activity of a Bioinspired Molecular CoII4O4 Cubane? An In-Depth Exploration of Catalytic Pathways. *ACS Catal.* **2016**, *6*, 1505−1517.
(84) Ezhov, R.; Ravari, A. K.; Bury, G.; Smith, P. F.; Pushkar, Y. Do multinuclear 3d metal catalysts achieve O−O bond formation via radical coupling or via water nucleophilic attack? WNA leads the way in [Co4O4]n+. *Chem. Catal.* **2021**, *1*, 407−422.
(85) Li, S.; Zhang, Z.; Marks, W. R.; Huang, X.; Chen, H.; Stoian, D. C.; Erni, R.; Triana, C. A.; Patzke, G. R. Co4O4 Cubanes in a conducting polymer matrix as bio-inspired molecular oxygen evolution catalysts. *Nat. Commun.* **2024**, *15*, 8432.
(86) Fenton, H. J. H. LXXIII.−Oxidation of tartaric acid in presence of iron. *J. Chem. Soc., Trans.* **1894**, *65*, 899−910.
(87) Haber, F.; Weiss, J. The catalytic decomposition of hydrogen peroxide by iron salts. *Proc. R. Soc. A* **1934**, *147*, 332−351.
(88) Kochi, J. K. The mechanism of the copper salt catalysed reactions of peroxides. *Tetrahedron* **1962**, *18*, 483−497.
(89) Kochi, J. K. The Decomposition of Peroxides Catalyzed by Copper Compounds and the Oxidation of Alkyl Radicals by Cupric Salts. *J. Am. Chem. Soc.* **1963**, *85*, 1958−1968.
(90) Lande, S. S.; Kochi, J. K. Formation and oxidation of alkyl radicals by cobalt(III) complexes. *J. Am. Chem. Soc.* **1968**, *90*, 5196−5207.
(91) Amtawong, J.; Skjelstad, B. B.; Balcells, D.; Tilley, T. D. Concerted Proton−Electron Transfer Reactivity at a Multimetallic Co4O4 Cubane Cluster. *Inorg. Chem.* **2020**, *59*, 15553−15560.
(92) Shimoyama, Y.; Kojima, T. Metal−Oxyl Species and Their Possible Roles in Chemical Oxidations. *Inorg. Chem.* **2019**, *58*, 9517−9542.
(93) Yang, J.; Dong, H. T.; Seo, M. S.; Larson, V. A.; Lee, Y.-M.; Shearer, J.; Lehnert, N.; Nam, W. The Oxo-Wall Remains Intact: A Tetrahedrally Distorted Co(IV)−Oxo Complex. *J. Am. Chem. Soc.* **2021**, *143*, 16943−16959.
(94) Sen, A.; Sharma, S.; Rajaraman, G. Bridging the Oxo Wall: A New Perspective on High-valent Metal-Oxo Species and Their Reactivity in Mn, Fe, and Co Complexes. *Angew. Chem., Int. Ed.* **2025**, *64*, e202419953.
(95) Denisov, E. T.; Denisova, T. G. Oxidation of alcohols involving two types of peroxyl radicals. *Pet. Chem.* **2006**, *46*, 305−313.
(96) Zhou, L.; Yu, D.; Wang, Z.; Cheng, L.-J.; Jin, Z.-H.; Weng, J.-J.; Yang, J.-Z.; Tian, Z.-Y. A detailed kinetic study on oxidation of benzyl alcohol. *Combust. Flame* **2019**, *207*, 10−19.
(97) Han, Q.; Zhou, X.-T.; He, X.-Q.; Ji, H.-B. Mechanism and kinetics of the aerobic oxidation of benzyl alcohol to benzaldehyde catalyzed by cobalt porphyrin in a membrane microchannel reactor. *Chem. Eng. Sci.* **2021**, *245*, 116847.
(98) Saussine, L.; Brazi, E.; Robine, A.; Mimoun, H.; Fischer, J.; Weiss, R. Cobalt(III) alkylperoxy complexes. Synthesis, x-ray structure, and role in the catalytic decomposition of alkyl hydroperoxides and in the hydroxylation of hydrocarbons. *J. Am. Chem. Soc.* **1985**, *107*, 3534−3540.
(99) Talsi, E. P.; Chinakov, V. D.; Babenko, V. P.; Sidelnikov, V. N.; Zamaraev, K. I. Role of alkylperoxo complexes of cobalt (III) in catalytic oxidation of cyclohexane by cumene hydroperoxide in the presence of bis (acetylacetonato) cobalt (II). *J. Mol. Catal.* **1993**, *81*, 215−233.
(100) Chavez, F. A.; Mascharak, P. K. Co(III)−Alkylperoxo Complexes: Syntheses, Structure−Reactivity Correlations, and Use in the Oxidation of Hydrocarbons. *Acc. Chem. Res.* **2000**, *33*, 539−545.

Downloaded from pubs.acs.org/inocaj/article-pdf/doi/10.1021/acs.inorgchem.6c03033/6828356/acs.inorgchem.6c03033.pdf by RUHR UNIVERSITAET BOCHUM user on 03 September 2026

https://doi.org/10.1021/acs.inorgchem.6c03033
Inorg. Chem. XXXX, XXX, XXX−XXX